Article

Crystal engineering of pharmaceutical co-crystals: "NMR- crystallography" of Niclosamide co-crystals

David Luedeker, Rebecca Gossmann, Klaus Langer, and Gunther Brunklaus

Cryst. Growth Des., **Just Accepted Manuscript** • DOI: 10.1021/acs.cgd.5b01619 • Publication Date (Web): 19 Apr 2016

Crystal engineering of pharmaceutical co-crystals: "NMR-crystallography" of Niclosamide co-crystals

David Luedeker,[†] Rebecca Gossmann,[‡] Klaus Langer,[‡] and Gunther Brunklaus*[,†]

[†]Institut für Physikalische Chemie, Westfälische Wilhelms-Universität Münster, Corrensstr. 28, D-48149 Münster, Germany

Fax: (+49)-251-83-36032; email: gbrunklaus@uni-muenster.de

[‡]Institut für Pharmazeutische Technologie und Biopharmazie, Westfälische Wilhelms-Universität Münster, Corrensstr. 48, D-48149 Münster, Germany

Abstract: Niclosamide is a Biopharmaceutics Classification System (BCS) class II taeniacide currently reconsidered for new promising applications including treatment of rheumatoid arthritis, prevention of protein degeneration in neurodegenerative diseases or even multi-targeted therapy of cancer and cancer stem cells. Its efficacy in medical treatments, however, is currently limited by its insufficient solubility or bioavailability. Thus we have further explored the potential of hydrogen-bond mediated co-crystal formation of niclosamide with suitable co-formers selected from either the "Generally Regarded as Safe" (GRAS) or United States Food and Drug Administration (US FDA) "Everything Added to Food in the United States" (EAFUS) list, respectively. Solvent-assisted solid grinding and/or slow solvent evaporation yielded four new co-crystals: (i) niclosamide – 2-aminothiazole (NCL-AT), (ii) niclosamide – benzamide (NCL-BA), (iii) niclosamide – isoniazide (NCL-IN), and (iv) niclosamide – acetamide I and II (NCL-AA-I/NCL-AA-II). The crystal structures of NCL-AA-I/II, NCL-AT were solved from white micro-crystalline powder samples based on the combined application of powder X-ray diffraction (PXRD), solid-state NMR and Density Functional Theory (DFT) chemical shift computation. In addition, the crystal structure of the monohydrate NCL-H_A was reconsidered for comparison. Finally an improvement of the equilibrium solubility of the (1:1) co-crystal NCL-AT could be determined (2.8x that of pristine NCL and 1.4x that of NCL-UREA co-crystal), suggesting NCL-AT as a candidate for future medical treatment.

Keywords

NMR crystallography, niclosamide, pharmaceutical co-crystal, PXRD structure solution, polymorphism, niclosamide hydrate, niclosamide co-crystal.

1. Introduction

Niclosamide (2', 5-dichloro-4'-nitrosalicylanilide, NCL) is a hydrophobic taeniacide and restricted-use pesticide that may be applied to cure parasite infestations (including most tapeworms and cestoda)[1] in both humans and animals or for water treatment against e.g. sea lampreys (*Petromyzon marinus*)[2] or apple snails (*Pomacea canaliculata*).[3] Its primary effect comprises the inhibition of energy production in mitochondria,[4] though NCL may also bind to DNA after its reductive activation[5] rendering it possibly toxic to some aquatic organisms or plants.[6] An early long term toxicology survey of molluscicides indicated that NCL neither has increased mutagenic, oncogenic or embryotoxic activity nor impact on liver and kidney functions.[7] Despite that a single oral dose of NCL for adults in cestocidal treatment amounts to 2 g,[8] NCL exhibits a very low acute toxicity in humans[9] reflecting both its insufficient oral bioavailability (merely 10% in male Sprague-Dawley rats)[10] and the fact that NCL is poorly absorbed from the intestinal tract.[11] However, in view of recently identified promising properties of NCL such as anti-inflammatory effects useful for the treatment of rheumatoid arthritis,[12] the prevention of protein aggregation in neurodegenerative diseases[13] or even for multi-targeted therapy of cancer and cancer stem cells[14] (including an application of NCL as effective radio-sensitizer),[15] research efforts are currently devoted to considerably improve the solubility (and thus bioavailability) of NCL thereby enhancing the achievable maximal serum concentrations and its efficacy in medical treatments.

In addition to suitable drug carriers such as polymeric particles[16-18] or even supramolecular hosts[19-21] introduced during formulation, either efficient *crystallization* screening (including polymorphs, salts, solvates or co-crystals)[22-24] or tailored *amorphization* of the active drug[25-28] or its multi-component system of interest (co-amorphous drug systems)[29] constitute two major approaches that are available for the manipulation of physicochemical properties of drugs. Though amorphous drugs may have great potential to reduce issues related to either poor dissolution rate or solubility-limited absorption in particular in case of drugs where salt formation cannot be applied, this approach is not readily accessible for the non-glass former NCL.[30] Therefore, the various attempts to counteract NCLs hydrophobic nature in order to facilitate better aqueous dispersion or solubility of NCL for example include salt formation of NCL with either ethanolamine[31] or sodium (as part of a polymer-based controlled-release formulation)[32] and inclusion of NCL in 4-sulphonatao-

calix[n]arene[33] or cyclodextrin[34] host systems. Since the NCL delivery formulations were mainly considered in the framework of water treatment such as control of snails in farm fields neither compatibility nor toxicity of certain additives with respect to the human metabolism was explicitly evaluated which only recently has changed due to the emerging interest in NCL as a potential candidate in cancer therapy.[35] Consequently, chemically modified but highly water soluble derivatives of NCL, (e.g. with an attached phosphate group[36] or alkylamino tethered derivatives[37]) have been introduced, though at the expense of rather tedious synthetic protocols.

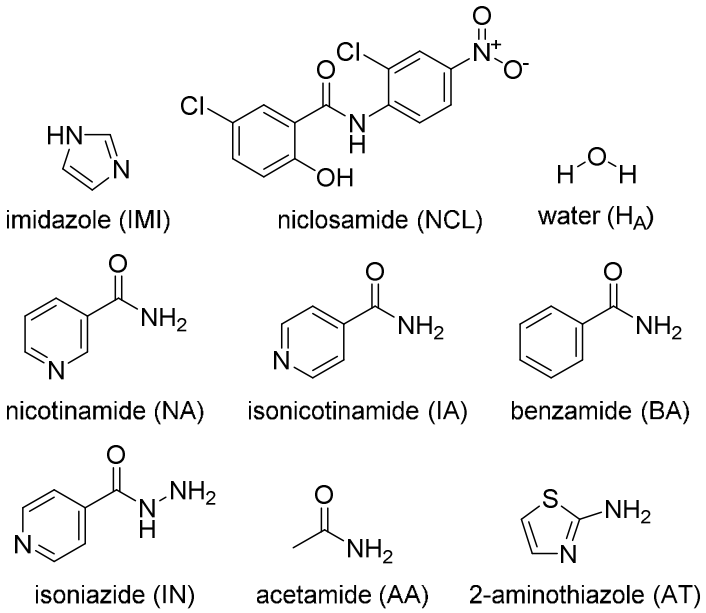

Figure 1: *The molecular structures of niclosamide and the considered co-formers discussed in this study. All obtained co-crystals of niclosamide and the monohydrate NCL-H_A have a (1:1) stoichiometry. Note that the crystal structure of NCL-H_A was very recently reported[38] and is reconsidered for comparison, while 2-aminothiazole derivatives were suggested as therapeutic leads for the treatment of prion diseases.[39]*

Moreover, the concept of hydrogen-bond mediated formation of *pharmaceutical co-crystals*[40-46] was successfully applied to obtain co-compounds of NCL with suitable molecules taken from either the "Generally Regarded as Safe" (GRAS) or US FDA "Everything Added to Food in the United States" (EAFUS) list[47] including caffeine (CAF), urea (URE), *p*-amino-benzoic acid (PABA), theophylline (THPH), nicotinamide (NA) or isonicotinamide (IA), respectively.[48] The co-crystals were designed according to the availability of specific supramolecular synthons[49-51] and are mainly based on the robust {OH···O} synthon though in case of *para*-amino-benzoic acid the {OH···NH_2} synthon was identified. Since nicotinamide and its stereoisomer isonicotinamide contain $CONH_2$ and $N_{aromatic}$ functional groups, the likely resulting co-crystals may exhibit {OH···O}, {OH··

·NH_2}, or {OH···$N_{aromatic}$} synthons where the latter is a particularly versatile supramolecular unit for crystal engineering applications.[52-54] In addition, salt co-crystals with concomitant presence of NCL both as neutral component and as salt co-former (derived from salification of NCL with inorganic salts) as well as mixed solvate/hydrate salts of NCL were very recently reported.[55] The latter partially included the solvent dimethyl sulfoxide (DMSO), which in view of the identified brain degeneration due to apoptosis in the central nervous system induced by DMSO already at low doses of 0.3 mL/kg appears pharmaceutically questionable.[56] Therefore, the intent of this work was to further explore the reliability of hydrogen-bond mediated co-crystal formation for the improvement of the solubility of NCL considering suitable co-former molecules that contain either amide groups and/or aromatic nitrogen atoms, respectively (Figure 1). From solvent assisted solid grinding and/or slow solvent evaporation new co-crystals of (i) niclosamide – 2-aminothiazole (NCL-AT), (ii) niclosamide – benzamide (NCL-BA), (iii) niclosamide – isoniazide (NCL-IN) and the polymorphic system (iv) niclosamide – acetamide I and II (NCL-AA-I/ NCL-AA-II) were successfully prepared. Since structure solutions were not yet provided in case of the co-crystals of NCL-NA (vi), NCL-IA (vii), niclosamide – imidazole (NCL-IMI), respectively, these co-compounds were reproduced for further structural characterization. However, in the absence of single crystals suitable for single-crystal X-ray diffraction, the corresponding crystal structures of both NCL-AA-I/II and NCL-AT were solved from micro-crystalline powdered samples based on the combined application of powder X-ray diffraction (PXRD), solid-state NMR and Density Functional Theory (DFT) chemical shift computations, an approach that we have recently applied for the structure solution of co-crystals of ezetimibe with imidazole and L-proline.[57] Briefly, the currently evolving concept of "NMR crystallography"[58-64] comprises at least the two-step strategy of an initial structure model derived from either powder diffraction techniques[65,66] or where feasible from crystal structure prediction (CSP)[67-69] and subsequent structure validation against experimental data, often including solid state NMR chemical shifts or chemical shift tensor data, respectively, that are computed by DFT methods based on the proposed structure models (or identified building blocks) where the best match indicates the (apparently) most likely crystal structure.[70-76] Besides, the structural refinement may be supported by complementary data input obtained from solid state NMR such as the number of independent molecules in the asymmetric unit (Z´), molecular connectivity, or in particular characteristic distances extracted from dipolar couplings.[77-87] Experimental ^{1}H solid state NMR chemical shifts have even been utilized for immediate structure generation based on a genetic algorithm and

applied as pseudo-forces during structure refinement,[88] while in other cases the corresponding ^{1}H solid state NMR chemical shifts of protons involved in reasonably strong hydrogen bonding (depending on the actually considered synthon) could be correlated with the explicit geometry of the hydrogen bond thus allowing for an estimation of corresponding distances and/or torsion angles from solid state NMR data.[89-92] In an alternative approach, ^{13}C solid-state NMR data was applied to establish a crystal structure even in the absence of powder diffraction data and single crystals,[93] though such data more typically has been considered for structure validation or identification of molecular conformation or polymorphism present in solid materials.[94-97] Despite the presence of many distinct protocols (including software packages) the high versatility of the interdisciplinary concept of "NMR crystallography" to support solving or refinement of crystal structures of powdered solids is indeed convincingly demonstrated by a continuously growing number of contributions that report successful structure elucidation of a variety of materials.[98-109]

2. Results and Discussion

Rather well defined crystalline drugs are often preferred for the tailored design of solid oral dosage forms based on crystal engineering strategies.[110] Niclosamide, however, is prone to solvate, hydrate or mixed solvate/hydrate formation even when reacted under solvent assisted solid grinding where only a few drops of suitable solvent are present. Thus several solvates of NCL with methanol (MeOH);[111] acetone and acetonitrile;[38] dimethyl sulfoxide (DMSO), N,N'-dimethyl formamide (DMF), diethyl ether (Et_2O);[112] tetrahydrofuran (THF) and tetraethylene glycol (TEG);[113] and the polymorphic monohydrates NCL-H_A[38] and NCL-H_B[114,115] have been reported, thereby clearly emphasizing the necessity to utilize rather purified water-free solvents for the co-crystal synthesis of NCL to circumvent any hydrate by-products. While unintentional changes of the level of hydration or even complete dehydration of pharmaceutical solids ideally can be avoided during formulation development or manufacture under controlled conditions, this may be more difficult upon prolonged storage of the final product which then may adversely affect its physical, chemical or bio-medical properties.[116] Similarly, charge-assisted synthons formed due to salt formation tend to be hygroscopic and should be avoided as well rendering co-crystallization attempts based on neutral synthons such as {OH···O} or {NH···O} rather preferred. Note that in the abundant presence of different hydrogen-bond donor and acceptor moieties in a given crystal structure, the analysis of data sets from the Cambridge Structural Database (CSD) indicates that the

majority of hydrogen bond donors (particularly the strong donors) will be satisfied (and hence involved in hydrogen bonding) while a larger fraction of acceptors may remain "free".[117]

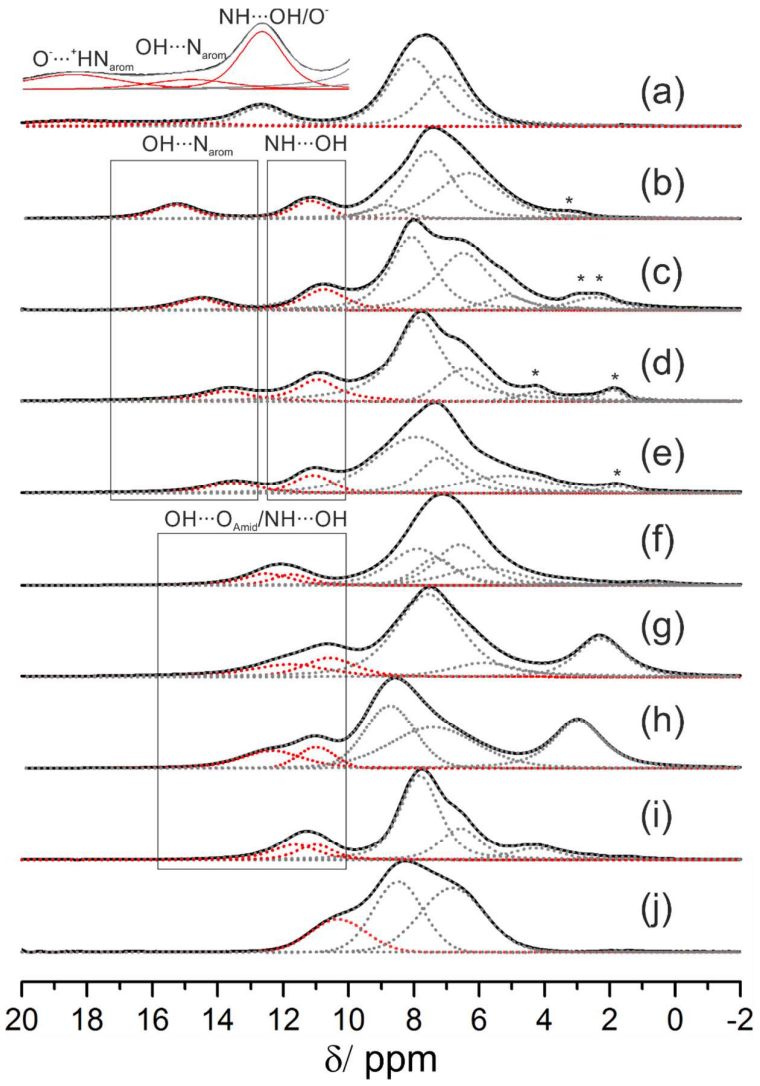

Figure 2: *^{1}H MAS NMR spectra (acquired at 500.1 MHz and 30 kHz spinning frequency) of (a) NCL-IMI, (b) NCL-AT, (c) NCL-IA, (d) NCL-NA, (e) NCL-IN, (f) NCL-BA, (g) NCL-AA-II, (h) NCL-AA-I, (i) NCL-H_A and (j) NCL anhydrate. The region for the NCL-IMI spectrum between 10-20 ppm is enlarged on top, while the signals attributed to small impurities from residual solvents (either ethanol or ethyl acetate) are marked by asterisks.*

Indeed, the molecular structure of NCL exhibits a planar, secondary amide group comprised of a C=O hydrogen bond acceptor and NH hydrogen bond donor. The latter forms an intramolecular S(6) hydrogen bonded ring with the oxygen atom of a neighboring hydroxyl group resulting in an exposed OH unit that may be considered as suitable hydrogen donor for the successful co-crystal and/or solvate formation of NCL, as documented in the pristine compound NCL where this hydroxyl group connects via intermolecular $C_1^1(6)$ chains with the carbonyl hydrogen bond acceptor of an adjacent NCL moiety (note that NCL crystallizes in

the monoclinic space group $P2_1/c$ with one molecule in the asymmetric unit). In order to enhance the probability of successful co-crystal formation of NCL, all of the selected co-former molecules offer a competitive hydrogen-bond acceptor such as other C=O units or aromatic nitrogen atoms (Figure 1) that upon either solvent assisted solid grinding or slow solvent evaporation typically yielded micro-crystalline powdered samples rather than single crystals.

Solid state MAS NMR. Successful formation of phases different from the starting materials was monitored by solid-state NMR which is applicable even in cases where possibly amorphous products would be obtained (particularly in early attempts where the reaction conditions are not suitably established). The spatial rearrangement of molecules including the coordination of the exposed OH (or even NH) group of NCL to a hydrogen bond acceptor of the offered co-former molecules result in different hydrogen bonding pattern compared to the precursor compounds, which depending on the strength or bond lengths (or even geometry) of the considered hydrogen bond is typically reflected by quite characteristic changes of the corresponding ^{1}H magic-angle spinning (MAS) NMR spectra (Figure 2).[118-120] Notably, based on the analysis of integrated area ratios extracted from deconvolution of experimental ^{1}H NMR spectra (peak fitting) particularly considering the signal fraction of sufficiently hydrogen bonded protons (e.g., NCL-OH or NCL-NH) to "ordinary" protons the molecular composition of the compound can be derived, allowing for a comparison with the intended stoichiometry. An inspection of the ^{1}H MAS NMR spectra of NCL-AT, NCL-IA, NCL-NA and NCL-IN (Figure 2(b)-2(e)), respectively, where the peaks of NCL-NH and NCL-OH are clearly separated, revealed integrated area ratios of 1:1:10 (NCL-AT), 1:1:12 (NCL-IA), 1:1:12 (NCL-NA) and 1:1:13 (NCL-IN), in addition to integrated area ratios of 1:1:13 (NCL-BA), 1:1:11 (NCL-AA-I, NCL-AA-II) and 1:1:8 (NCL-H_A) derived from peak fitting (Figure 2(f)-2(i)), which in all considered cases are in excellent agreement with a 1:1 stoichiometry of NCL and the corresponding co-former. This even holds for the compound NCL-IMI, based on the 3:9 integrated area ratio of hydrogen bonded protons (distributed in the region from 12.6 to 18.6 ppm) and aromatic protons. In most cases, the ^{1}H chemical shift of the NCL-NH group amounts to {11.0 – 11.7 ppm}, except for NCL-IMI (12.7 ppm) and NCL-URE (9.8 ppm), thus indicating that the planar conformation including the intramolecular S(6) hydrogen bonded ring of the NCL anhydrate structure (β-conformation) remained intact in the obtained co-crystals. This finding was further verified based on the corresponding ^{15}N chemical shift of {245.5 – 248.9 ppm}, in agreement with quite negligible changes of local electron density

distributions (Figure S1). In contrast, the ^{1}H NMR chemical shift of the exposed O–H group of NCL showed a strong dependence on the actually formed synthon upon co-crystallization, ranging from {11.0 – 12.3 ppm} and {13.5 – 15.3 ppm} for {O–H···O} and {O–H···N} hydrogen bonds, respectively. Note that the co-crystal NCL-AT is stabilized by rather strong {O–H···N} hydrogen bonds as reflected by a high ^{1}H chemical shift of 15.3 ppm for the NCL-OH group. Based on the observed ^{1}H chemical shifts of the co-crystals that contain aromatic nitrogen acceptors (including NCL-IN, NCL-NA and NCL-IA) whose crystal structures are not yet plausibly solved from the available PXRD pattern, it indeed can be concluded that the NCL-OH group coordinates to the aromatic nitrogen rather than amide or hydrazine groups of the co-former thereby yielding comparatively stronger hydrogen bonds.

In the case of linear hydrogen bonds with fixed donor (D) and acceptor (A) atom distances (e.g., O···O, O···N or N···N) the ^{1}H chemical shift of the proton is explicitly correlated with the position of the proton within the hydrogen bond where quite high ^{1}H chemical shielding (hence chemical shift) was attributed to either short D-H distances or "stretched" symmetric hydrogen bonds in which the proton approached the center of the D···A bond,[121] though the occurrence of charges due to proton transfer could also result in increased ^{1}H chemical shifts.[122] In principle the formation of a charge assisted synthon $\{_{NCL}O^{-}\cdots{}^{+}HN_{IMI}\}$ is feasible for NCL-IMI in addition to $\{_{NCL}NH\cdots{}^{-}O_{NCL}\}$ thereby shifting the peak of NCL-NH to higher ppm (12.7 ppm) compared to the neutral synthon $\{_{NCL}NH\cdots O_{H,NCL}\}$ that typically comprises the S(6) intramolecular ring of NCL. If the IMI-NH unit is also taken into account, it becomes clear why the integrated area ratio of hydrogen bonded to "ordinary" protons amounts to 3:9. A deconvolution of the ^{1}H MAS NMR spectrum of NCL-IMI revealed an integrated area ratio of 0.95:0.05:2 for the corresponding peaks at 18.5, 14.9 and 12.7 ppm, respectively, thus suggesting that the minor peak at 14.9 ppm represents an "impurity". In addition, the experimental data indicates that the resonances of both NCL-NH and IMI-NH incidentally coincide at 12.7 ppm if the peak at 18.5 ppm is tentatively attributed to IMI-NH^{+}. NCL-NH and IMI-NH should have different protons in their immediate spatial proximity which may be revealed based on characteristic correlation peaks in a 2D ^{1}H-^{1}H dipolar double-quantum (DQ) spectrum where so-called double-quantum coherences due to *pairs* of dipolar coupled protons are correlated with single-quantum (SQ) coherences.[123,124] DQ signals therefore appear at the *sum* of the chemical shifts of the coupled protons (facilitating the identification of sites obscured due to overlapping peaks) while the DQ signal intensities are proportional to r_{ij}^{-6} (the internuclear distance) hence yielding sufficient signal intensities only for those

protons in reasonable spatial proximity (distances of up to 4.0 Å). The DQ MAS NMR spectrum of NCL-IMI (Figure 3) exhibits two particularly revealing DQ peaks with significantly different intensities at 19.7 ppm (12.7 + 7.0 ppm, 11% of max. intensity) and 20.2 ppm (12.7 + 7.5 ppm, 4% of max. intensity) that reflect dipolar coupling to unlike aromatic protons (7.0 vs. 7.5 ppm), in good agreement with two *different* protons (NCL-NH and IMI-NH) coinciding at 12.7 ppm. In addition, a rather strong DQ (cross)peak at 31.2 ppm (12.7 + 18.5 ppm) is indicative of spatial proximity of NCL-NH (12.7 ppm) and IMI-NH^+ (18.5 ppm) whereas a DQ (auto)peak at 25.4 ppm (12.7 + 12.7 ppm) suggests molecular packing that result in similar proximity of NCL-NH (12.7 ppm) with NCL-NH (12.7 ppm) or IMI-NH (12.7 ppm) with IMI-NH (12.7 ppm), since a dipolar coupling of NCL-NH with IMI-NH (when considering likely distances) is rather unlikely to yield such a DQ signal.

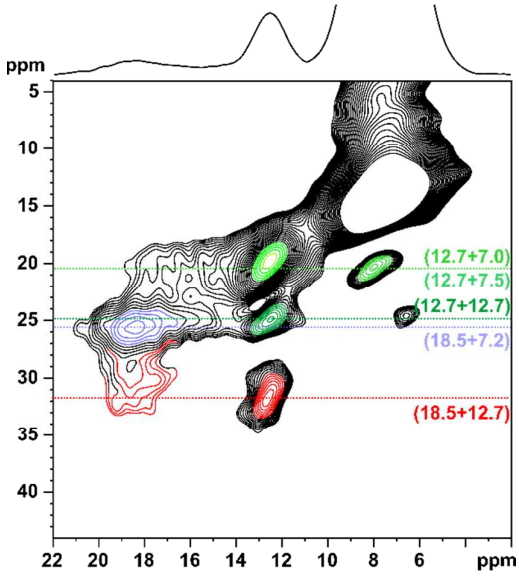

Figure 3: *^{1}H-^{1}H DQ-MAS-NMR spectrum of NCL-IMI, recorded at 500.1 MHz and 30 kHz MAS. 32 positive contour levels between 1% and 35% of the maximum peak intensity were plotted. The F2 projection is shown on top; the most important DQ cross-peaks are highlighted, illustrating that two different proton sites coincide at 12.7 ppm.*

Except for NCL-IMI, the ^{1}H-^{1}H DQMAS NMR spectra (Figures S12-S18) were primarily considered for structure validation with respect to the hydrogen bonding network present in the final structure solutions derived from Rietveld refinement, though independent distance constraints and hence insight into the molecular packing may be derived from DQ build-up curves (monitoring of DQ signal intensities as a function of DQ excitation times).[125,126] In addition to exploiting the integrated area ratio of the ^{1}H MAS NMR spectra to determine the ratio of the molecular constituents of the considered co-compound, the content of the asymmetric unit (which is an essential information with respect to the structure solution from

PXRD data) was estimated based on $^{15}N\{^{1}H\}$ (Figure S1) or $^{13}C\{^{1}H\}$ (Figure S2) cross-polarization MAS NMR spectra of the co-crystals, explicitly utilizing that all inequivalent atoms (those not generated by symmetry elements)[127] comprising a given structure result in individual NMR signals provided that sufficient spectral resolution could be achieved. Nevertheless, in case of hydrogen-bonded nitro groups (often if connected to aromatic rings) the occurrence of rotational dynamics may perturb the ^{1}H-^{15}N polarization transfer thereby rendering the corresponding ^{15}N signals eventually "invisible", irrespective of the applied cross-polarization contact time.[128,129] Most other nitrogen atoms could be identified including the unique IMI-NH^{+} at -213.7 ppm.

Powder X-ray Diffraction. In addition to the solid state NMR analysis, the powdered compounds derived from solvent-assisted grinding of stoichiometric mixtures of the precursor materials were investigated by powder X-ray diffraction. Indeed, successful formation of phases different from the starting materials could be readily identified form the occurrence of new peaks in the corresponding diffraction pattern and in due consideration of the available solid state NMR data were attributed to the formation of co-crystals. Notably, we have obtained the (1:1) co-crystals NCL-AT, NCL-IMI, NCL-AA, NCL-BA, NCL-IN as well as NCL-NA and NCL-IA while the monohydrate NCL-H_A[38] was reconsidered for comparison. Despite quite substantial efforts, attempts to grow larger crystals suitable for single-crystal XRD analysis from slow solvent evaporation were not successful so that structure solutions were derived from powder XRD data taking complementary structural input from solid state NMR data of the respective co-phases into account. An inspection of the PXRD pattern of the starting compound NCL anhydrate (Figure S3(a)) revealed that its most intense reflections are at 2Θ = {13.3°, 13.9°, 26.1°, 26.7° and 27.2°} so that changes of those peaks were indicative of the formation of new phases. For NCL-H_A the characteristic reflections are at 2Θ = {9.4°, 10.6°, 16.9°, 25.6° and 27.2°}[38] (Figure S4(b)) while major reflections at 2Θ = {10.4°, 13.1°, 22.4°, 26.8° and 27.3°} (Figure S4(c)) are identified in the theoretical XRD pattern computed from available single crystal structure data of NCL-H_B. Note that all three XRD pattern are significantly different from each other as indeed expected in the case of three independent phases. Likewise, the most significant new reflections for NCL-IMI at 2Θ = {6.1, 8.1, 16.3, 26.6 and 28.2} (Figure 4), for NCL-AT are at 2Θ = {7.0°, 9.4°, 15.8°, 26.4° and 27.6°} (Figure 6), for NCL-AA-I at 2Θ = {8.7°, 14.4°, 18.7°, 25.9°, and 26.6°} (Figure 8) and for NCL-AA-II at 2Θ = {6.1°, 8.8°, 17.7°, 19.6° and 26.5°} (Figure 9). Also, the co-crystals NCL-BA and NCL-IN yielded characteristic reflections at 2Θ = {5.6°, 8.0°, 12.2°, 16.7°, and 25.6°} (Figure S6(e)) and at 2Θ = {5.1°, 5.6°, 7.6°, 24.0° and 27.3°} (Figure S6(f)). The two

co-crystals NCL-IA and NCL-NA have been reproduced for further structural characterization since no explicit structure solution was provided in the original work.[48] Their most significant reflections are at: 2Θ = {5.4°, 7.7°, 13.9°, 27.0°, and 27.6°} (NCL-IA; Figure S3(d)) and 2Θ = {5.5°, 7.7°, 14.0°, 27.1°, and 27.6°}(NCL-NA; Figure S3(e)). The explicit structure solution in all considered cases started with profile fitting and indexing of the recorded PXRD pattern with both *N-TREOR* and *DICVOL04* as implemented in the *expo2014* and *DASH* software packages until reasonable solutions were obtained. The indexing attempts for the co-crystals NCL-NA, NCL-IA, NCL-BA and NCL-IN yielded rather flat unit cells that were similar to the unit cells of NCL-H_A, NCL-AA-II and NCL-MeOH, respectively.

Table 1: *Crystallographic parameters obtained for the crystal structures of the (1:1) co-crystals of NCL with imidazole (IMI), 2-aminothiazole (AT) and acetamide (AA), respectively. In case of NCL-H_A that was considered for comparison with NCL-H_B, the assignment of the crystal axes in our case was done purposely to demonstrate its structural relationship to NCL-H_B, preferring the space group $2_1/a$ over $2_1/c$, while the lattice parameters are similar to the reported structure of NCL-H_A.[38]*

	NCL-H_A	**NCL-IMI**	**NCL-AT**	**NCL-AA-I**	**NCL-AA-II**
emp. formula	$C_{13}H_{10}Cl_2N_2O_5$	$C_{16}H_{12}Cl_2N_4O_4$	$C_{16}H_{12}Cl_2N_4O_4S$	$C_{15}H_{13}Cl_2N_3O_5$	$C_{15}H_{13}Cl_2N_3O_5$
formula wt.	345.13	395.20	427.26	386.19	386.19
crystal system	monoclinic	monoclinic	monoclinic	triclinic	orthorhombic
space group	$P2_1/a$	$P2_1/c$	$P2_1/c$	P-1	$P2_12_12_1$
T/ K	295	295	295	295	295
a/ Å	23.05465(54)	4.02638(12)	12.89932(33)	11.21040(39)	20.00562(00)
b/ Å	16.15304(33)	21.80412(41)	18.77890(45)	11.01955(31)	21.20496(00)
c/ Å	3.812027(84)	19.30093(50)	7.44985(17)	7.57010(18)	3.88235(00)
α/ °	90	90	90	99.5245(25)	90
β/°	92.8243(23)	94.074(27)	99.6491(27)	103.1851(22)	90
γ/°	90	90	90	108.3846(23)	90
volume/ $Å^3$	1417.884(54)	1690.179(75)	1779.084(76)	835.026(47)	1647.964(00)
Z	4	4	4	2	4
Z'	1	1	1	1	1
radiation type, λ/ Å	Cu *K*α, 1.54060	Cu *K*α, 1.54060	Cu *K*α, 1.54060	Cu *K*α, 1.54060	Cu *K*α, 1.54060
R_{exp}	1.132	1.886	2.586	1.771	1.395
R_{wp}	1.977	2.579	4.227	6.351	6.235
R_p	1.415	1.826	3.327	4.155	4.431
GOF	1.747	1.412	1.634	3.587	4.470
χ^2	3.052	1.994	2.670	12.867	19.981
diffractometer	STOE StadiP	STOE StadiP	Bruker D8 Discover	Bruker D8 Discover	STOE StadiP

Niclosamide monohydrate H_A (NCL-H_A). The structure of the monohydrate NCL-H_A was independently solved in a monoclinic unit cell and space group suggested from a previous Le-Bail fit[111] similar to the recently reported crystal structure of NCL-H_A[38] except that the cell

axes *a* and *c* were exchanged for better comparability with the pseudo-polymorphic hydrate NCL-H_B. The structure solution converged quite quickly with excellent reproducibility within 50 consecutive *hybrid big bang big crunch* (HBB-BC) runs as implemented in *expo2014*, where the final refinement (Figure S8) gave an excellent goodness of fit (GOF = 1.747) and R_{wp} of 1.977 %. In our case, NCL-H_A crystallizes in the monoclinic space group $P2_1/a$ (No. 14) with one molecule of NCL and one molecule of water in the asymmetric unit (Z' = 1). Briefly, the NCL-OH group is hydrogen-bonded to one molecule of water that itself is coordinated to two other NCL moieties, while the S(6) ring involving NCL-NH is maintained (Figure S9).[38] Note that the rather short *c*-axis of the unit cell evokes π–π stacking of identical layers (at a stacking distance of 3.812 Å), similar but not isostructural to the known solvate of NCL with methanol,[111] while the trimeric coordination observed in NCL-H_A is also present in the crystal structure of the thermodynamically stable hydrate NCL-H_B. The comparison of the unit cells of both hydrates (NCL-H_A: $P2_1/a$, a ≈ 23.054(7) Å, b ≈ 16.153(0) Å, c ≈ 3.812(0) Å, β ≈ 92.824(3)°; H_B: $P2_1/c$, a = 11.332(2) Å, b = 16.964(2) Å, c = 7.346(3) Å, β = 98.281(2)°) indicates that the *a*-axis is approximately halved while the c-axis is doubled through the transformation from hydrate H_A to H_B, resulting in much less efficient π-π stacking in H_B. It therefore appears feasible that the π-π stacking of NCL is responsible for the crystallization of the kinetically favored hydrate H_A.

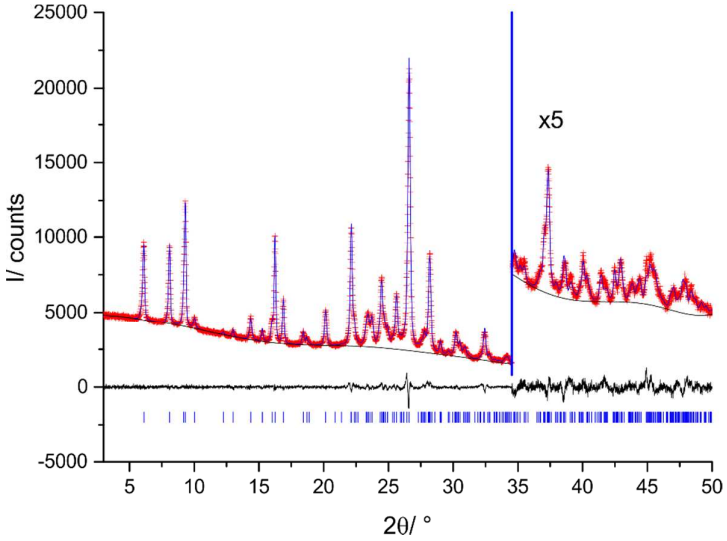

Figure 4: *The final Rietveld fit obtained for NCL-IMI: experimental data points (red), Rietveld refinement fit (blue), background (black line), difference I_{obs} - I_{calc} (black) and phase tick marks (blue). The vertical blue line marks the place at which the data points are multiplied with factor five for better visibility of the data in the higher 2Θ region.*

Niclosamide – imidazole (NCL-IMI). The crystal structure of NCL-IMI was solved in the monoclinic space group $P2_1/c$ (No. 14) with one molecule of NCL and one molecule of IMI in the asymmetric unit, in agreement with the solid state NMR data, where the structure solution converged with good reproducibility within consecutive *hybrid big bang big crunch* (HBB-BC) runs. The final Rietveld refinement (Figure 4) gave an excellent fit of the experimental PXRD pattern (GOF = 1.412) and R_{wp} of 2.579%. As before, the S(6) ring (1.739 Å, 137.6°) remained intact upon co-crystal formation. Based on the observation that all hydrogen bonded protons are shifted to higher ppm in the ^{1}H MAS NMR spectrum of NCL-IMI, the presence of an imidazolium ion is assumed, connecting two molecules of NCL via a charge-assisted {N–H$^+$···$^-$O} (1.613 Å, 157.1°) and a neutral {N–H···O} (2.223 Å, 132.7°) synthon, thereby leading to the formation of $C_2^2(10)$ chains which constitute layers. The obtained unit cell is relatively flat and stabilized by π–π stacking (4.026 Å), (Figure 5).

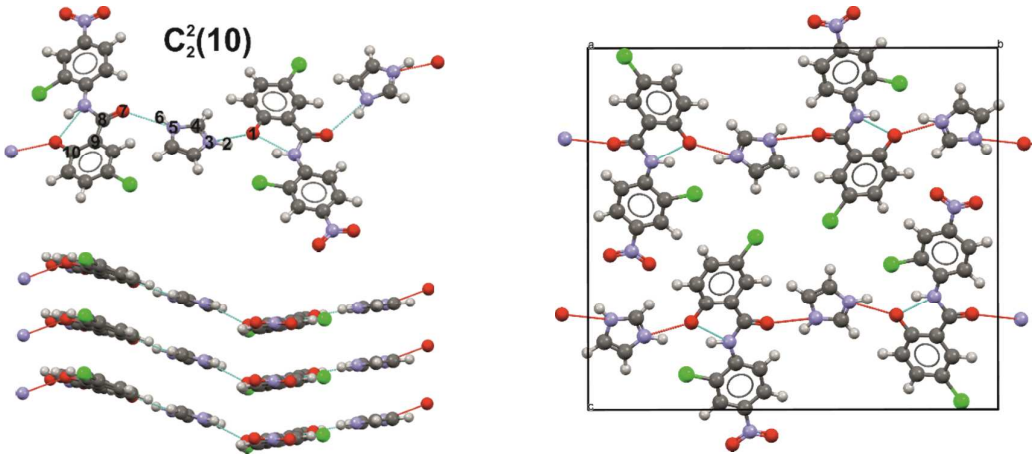

Figure 5: *(top left) The NCL-IMI (1:1) salt comprises a $C_2^2(10)$ chain formed by the deprotonated hydroxyl group of NCL and the aromatic NH^+ group of IMI as well as both the NH group of IMI and carbonyl oxygen of NCL, respectively; (bottom left) π–π interactions (at a distance of 4.026 Å) result in AAA packing of layers along the c-axis; (right) unit cell of the crystal structure viewed in the ab-plane.*

Niclosamide – 2-aminothiazole (NCL-AT). The structure of the (1:1) co-crystal NCL-AT was solved in the monoclinic space group $P2_1/c$ (No. 14) with one molecule of NCL and one molecule of 2-aminothiazole comprising the asymmetric unit, in agreement with the ^{1}H MAS NMR spectrum. As for NCL-H_A, the refinement converged quickly with a good reproducibility in repeated HBB-BC runs. The final Rietveld refinement (Figure 6) provided an excellent goodness of fit (GOF = 1.634) and R_{wp} of 4.227 %. It was found that the intramolecular {N–H···O} hydrogen bond of NCL (1.747 Å, 140.7°) persisted in the obtained co-crystal, while 2-aminothiazole links two molecules of NCL via $C_2^2(10)$ chains, including a rather strong intermolecular {O–H···N} hydrogen bond (1.587 Å, 170.6°) of the hydroxyl

group of NCL to an aromatic nitrogen of 2-aminothiazole and intermolecular {N–H···O} hydrogen bond (2.027 Å, 174.8°), connecting the amino group of 2-aminothiazole to the amide oxygen of NCL. The molecules are arranged in ABAB packing fashion along the *c*-axis through π–π stacking (3.645 Å) resulting in a *γ*-motif (Figure 7).

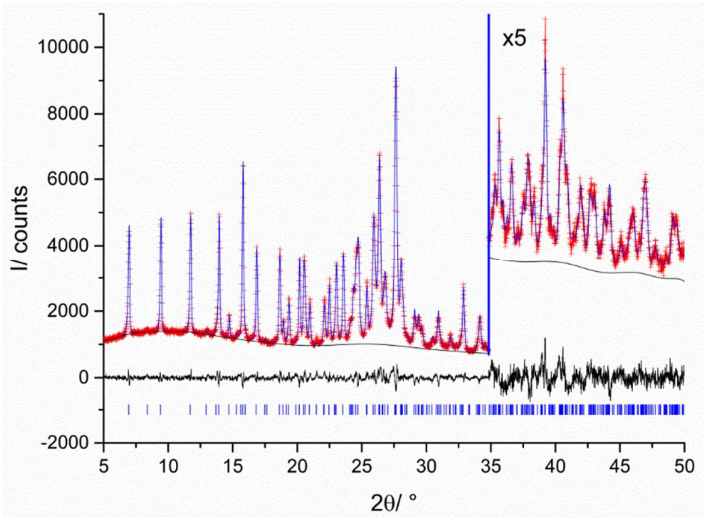

Figure 6: *The final Rietveld fit obtained for NCL-AT: experimental data points (red), Rietveld refinement fit (blue), background (black line), difference I_{obs} - I_{calc} (black) and phase tick marks (blue). The vertical blue line marks the place at which the data points are multiplied with factor five for better visibility of the data in the higher 2Θ region.*

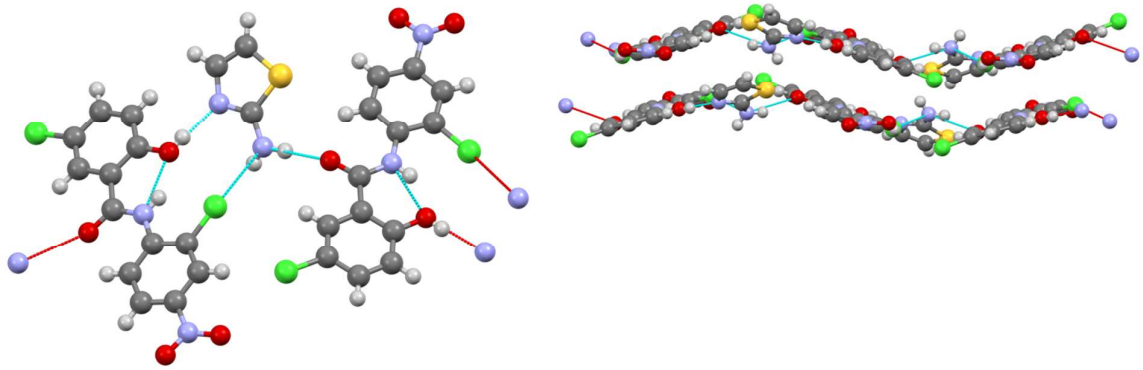

Figure 7: *(left) The NCL-AT (1:1) co-crystal comprises a $C_2^2(10)$ chain motif formed by the hydroxyl group of NCL and the aromatic nitrogen of 2-aminothiazole as well as both the amino group of 2-aminothiazole and carbonyl oxygen of NCL, respectively; (right) π–π interactions (at a distance of 3.645 Å) lead to ABAB packing of layers along the c-axis forming a γ-motif.*

Niclosamide – acetamide. Based on PXRD and solid-state NMR data it was identified that the co-crystallization of NCL and acetamide in all considered cases yielded polycrystalline mixtures of at least *two* polymorphs. Using a few drops of ethanol during solvent assisted solid grinding resulted in compound NCL-AA-I as dominating phase while in case of acetone NCL-AA-II was found as the main product. Nevertheless, since no experimental condition could be established that would result in pure co-crystal phases (e.g., only NCL-AA-I or

NCL-AA-II), multiphase Rietveld refinements were performed after independent structure solutions of NCL-AA-I and NCL-AA-II were achieved with sufficient reproducibility in the HBB-BC runs.

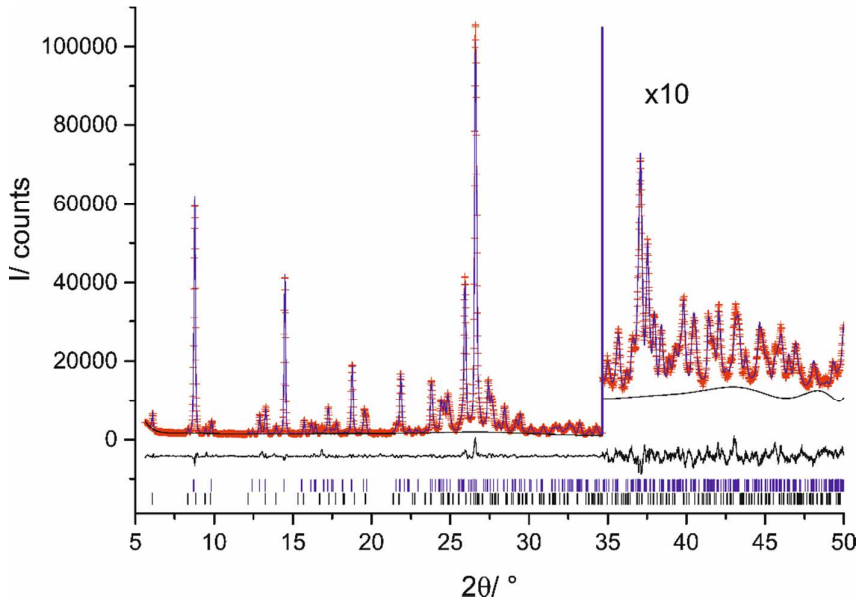

Figure 8: *The final Rietveld fit of the co-crystal polymorph NCL-AA-I: experimental data points (red), Rietveld refinement fit (blue), background (black line), difference I_{obs} - I_{calc} (black), phase tick marks of NCL-AA-I (blue) and phase tick marks of NCL-AA-II (black). The vertical blue line marks the place at which the data points are multiplied with factor ten for better visibility of the data in the higher 2Θ region.*

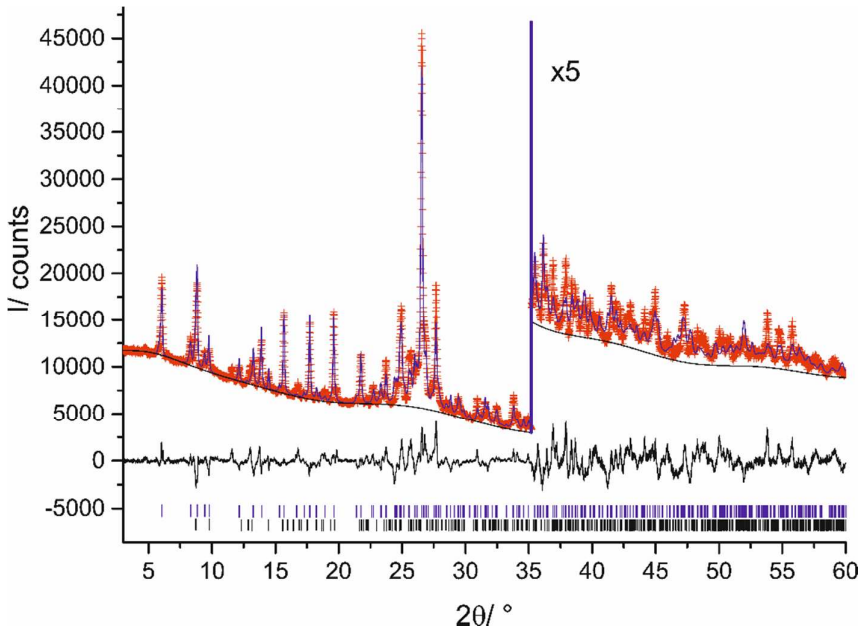

Figure 9: *Final Rietveld fit of the co-crystal polymorph NCL-AA-II: experimental data points (red), Rietveld refinement fit (blue), background (black line), difference I_{obs} - I_{calc} (black), phase tick marks of NCL-AA-II (blue) and phase tick marks of NCL-AA-I (black). The vertical blue line marks the place at which the data points are multiplied with factor five for better visibility of the data in the higher 2Θ region.*

The Rietveld refinement yielded quite acceptable values for both NCL-AA-I (GOF = 3.587, R_{wp} = 6.351 %; Figure 8) and NCL-AA-II (GOF = 4.470, R_{wp} = 6.235 %; Figure 9), though the overall quality of the refinement for NCL-AA-II is rather moderate. The corresponding fraction of impurity through the presence of the other polymorph could be quantified. In case of NCL-AA-I, a fraction of 13.5% NCL-AA-II was found while the co-crystal of NCL-AA-II contained a fraction of 6.6% NCL-AA-I. Notably, a comparison of the cell parameters of both NCL-AA-I and II revealed that the polymorphs are comparable to the hydrates NCL-H_A and NCL-H_B, respectively, though upon transformation of NCL-AA-II into NCL-AA-I the symmetry is lowered from an orthorhombic to a triclinic cell. Hence, the cell axes *a* and *b* are nearly halved whereas the *c*-axis is doubled so that in total the unit cell content is halved (NCL-AA-I: Z = 2; NCL-AA-II: Z = 4). As previously observed for the pseudo-polymorphic hydrates NCL-H_A and NCL-H_B, the π–π stacking in NCL-AA-II (AAA layers) seems to be more efficient than in NCL-AA-I (ABA layers) while the overall crystal packing is more efficient in NCL-AA-I.

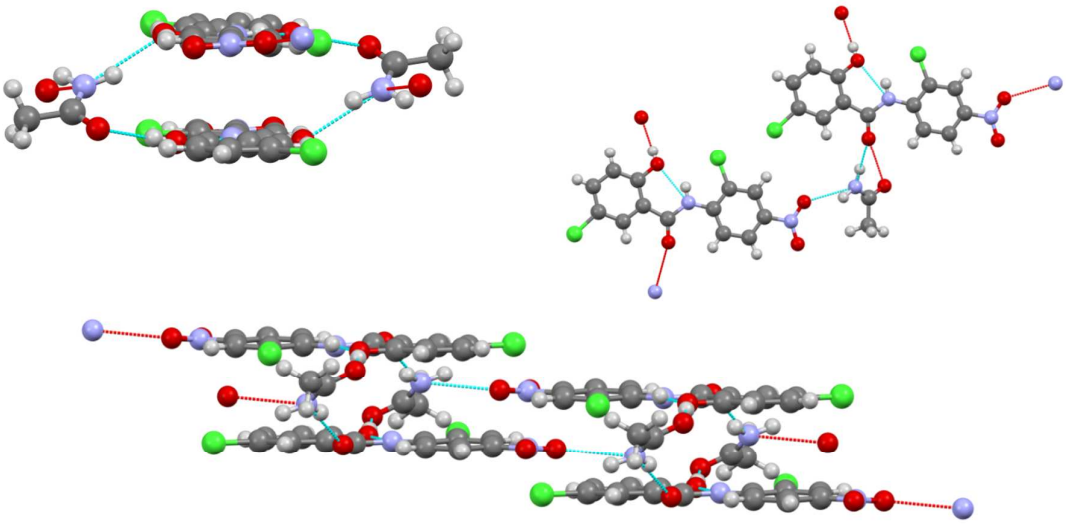

Figure 10: *(left top) The NCL-AA-I (1:1) co-crystal comprises a $R_4^4(20)$ ring motif between carbonyl oxygen of NCL and the amide group of acetamide connect ABAB layers of niclosamide. (right top) Within each layer of niclosamide molecules $C_2^2(12)$ chains link acetamide and NCL through the nitro group and carbonyl oxygen of NCL and the amide group of acetamide. (bottom) Two antiparallel acetamide ribbons form a column in which NCL molecules are stacked through π–π interactions at a distance of 3.404 Å.*

Niclosamide – acetamide I (NCL-AA-I). The (1:1) co-crystal NCL-AA-I crystallizes in the triclinic space group *P*-1 (No. 2) with one molecule of NCL and acetamide in the asymmetric unit. Acetamide links two different layers of NCL via a $R_4^4(20)$ ring (reminiscent of the NCL-

urea co-crystal) through {O–H···O} hydrogen bonds (1.694 Å, 176.4°) of NCL-OH and amide oxygen of acetamide as well as {N–H···O} hydrogen bonds (1.933 Å, 161.7°) of acetamide to the amide oxygen of NCL. Within one layer acetamide links NCL molecules through $C_2^2(12)$ chains over an {N–H···O} hydrogen bond (2.161 Å, 137.4°) to the nitro group and {N–H···O} hydrogen bond to the amide group of NCL, respectively. NCL molecules are connected to the next layer by π–π stacking (at a distance of 3.404 Å) along the *c*-axis in an ABAB fashion (Figure 10).

Niclosamide – acetamide II (NCL-AA-II). The polymorph NCL-AA-II crystallizes in the orthorhombic space group $P2_12_12_1$ (No. 19) with one molecule of both NCL and acetamide in the asymmetric unit (Figure 11). Acetamide forms infinite columns according to $C_1^1(4)$ chains through {N–H···O} hydrogen bonds (2.050 Å, 157.0°). The acetamide columns link two crossing layers of NCL along the *c*-axis via $D_2^3(7)$ hydrogen bonding motifs at which the hydroxyl group of NCL coordinates the oxygen of acetamide through {O–H···O} hydrogen bonds (1.756 Å, 175.5°). In addition the amide group of AA coordinates the nitro-group of NCL {N–H···O} so that as all donors and acceptors are saturated (1.987 Å, 142.3°). The NCL molecules build two columns that are placed diagonally to each other along the *c*-axis; within the columns the NCL molecules are connected via π–π stacking (3.882 Å) in AAA fashion, similarly to the case of the pseudo-polymorph NCL-H_A (Figure 11).

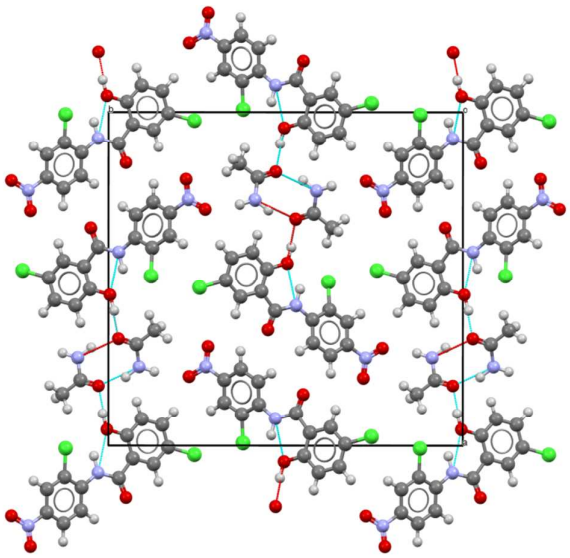

Figure 11: *The unit cell of the crystal structure of polymorph NCL-AA-II (viewed in the ab plane). The structure comprises $D_2^3(7)$ hydrogen bonding motifs between NCL-OH and the oxygen of AA that is part of $C_1^1(4)$ columns, while NCL layers are linked via π–π stacking (3.882 Å) in AAA fashion.*

Structure validation & DFT calculations. The evaluation of the correctness of structure solutions derived from profile fitting and analysis of PXRD pattern may be challenging without the input of complementary data. Therefore, structure solutions resulting from the final Rietveld refinement were subjected to DFT chemical shift computations where representative fragments ("cutouts") including important hydrogen bonding pattern and packing features (close contacts) of the considered structure were taken into account. Since reasonable structural models with well localized heavier atoms ("skeleton") are typically derived from PXRD data,[65,66] merely proton positions were optimized prior DFT NMR chemical shift computations. While this may not be suitable to tackle long-ranged van-der-Waals interactions among ordered aliphatic chains or cooperative π–π stacking effects in extended lattices or full periodic boundary conditions, the achievable accuracy in ^{1}H and ^{13}C chemical shifts of ±1 and ±(5-6) ppm at PBE/6-311G(d,p) level of theory[57,130] reflecting rather localized effects effectively allows a discrimination of different structural models at affordable computational costs. Though improved accuracy may in principle be expected from using higher basis sets and/or polarization functions, benchmark computations on a variety of molecules have revealed that this is not always the case, rendering the chosen level of theory a suitable compromise among the conflicting demands of required accuracy and computational costs.[131,132]

Table 2: *Experimental and DFT calculated ^{1}H chemical shifts of characteristic hydrogen bonds that stabilize the structures of the considered NCL hydrates and co-crystals. The superscript DQ denotes for the estimation of single quantum coherences from ^{1}H-^{1}H DQ MAS NMR data, provided that they could be unambiguously determined (if not, a '?' is set). Co-crystals for which no structure solution was obtained are marked with 'n.s.' (no structure).*

Phase	**H-bond motif**	**^{1}H, δ_{iso} (DFT)/ ppm**	**^{1}H, δ_{iso} (exp)/ ppm**	**d(X-H···Y)/ Å**	**Angle/ °**
NCL-H$_A$	$_{NCL}$O-H···O	11.1	11.0^{DQ}	1.742	168.6
	$_{NCL}$N-H···OH$_{NCL}$	11.6	11.6^{DQ}	1.717	140.5
	$_{H2O}$O-H···O$_{ket}$	5.5	*?*	1.803	176.6
	$_{H2O}$O-H···O$_{nitro}$	3.8	4.3^{DQ}	2.063	168.1
NCL-H$_B$	$_{NCL}$O-H···O	12.6	11.6[55]	1.616	171.9
	$_{NCL}$N-H···OH$_{NCL}$	11.9	11.6[55]	1.747	140.1
	$_{H2O}$O-H···O$_{ket}$	4.7	4.6[55]	1.891	168.6
	$_{H2O}$O-H···O$_{nitro}$	4.8	4.6[55]	1.981	168.0
NCL-AT	$_{NCL}$O-H···N$_{arom}$	15.7	15.3	1.587	170.6
	$_{NCL}$N-H···OH$_{NCL}$	11.7	11.2	1.747	140.7
	$_{AT}$N-H···O$_{NCL}$	7.8	7.1^{DQ}	2.027	174.8
	$_{AT}$N-H···O$_{NCL}$	5.7	5.7^{DQ}	2.271	160.4

NCL-AA-I	$_{NCL}$O-H···O	11.7	12.3	1.694	176.4
	$_{NCL}$N-H···OH$_{NCL}$	11.0	11.0	1.810	139.4
	$_{AA}$N-H···O$_{ket}$	8.4	*?*	1.933	161.7
	$_{AA}$N-H···O$_{nitro}$	7.4	*?*	2.161	137.4
NCL-AA-II	$_{NCL}$O-H···O	11.5	11.8	1.756	175.5
	$_{NCL}$N-H···OH$_{NCL}$	11.4	10.6	1.780	140.5
	$_{AA}$N-H···O$_{ket}$	7.8	*?*	2.050	157.0
	$_{AA}$N-H···O$_{nitro}$	8.2	*?*	1.987	142.3
NCL-BA	$_{NCL}$O-H···O	n.s.	12.5	n.s.	n.s.
	$_{NCL}$N-H···OH$_{NCL}$	n.s.	11.7	n.s.	n.s.
NCL-IN	$_{NCL}$O-H···N$_{arom}$	n.s.	13.5	n.s.	n.s.
	$_{NCL}$N-H···OH$_{NCL}$	n.s.	11.1	n.s.	n.s.
NCL-NA	$_{NCL}$O-H···N$_{arom}$	n.s.	13.7	n.s.	n.s.
	$_{NCL}$N-H···OH$_{NCL}$	n.s.	11.0	n.s.	n.s.
NCL-IA	$_{NCL}$O-H···N$_{arom}$	n.s.	14.4	n.s.	n.s.
	$_{NCL}$N-H···OH$_{NCL}$	n.s.	10.7	n.s.	n.s.
NCL-IMI	$_{NCL}$O^{-}···$^{+}$HN$_{arom}$	17.9	18.5/ 18.2[55]	1.613	157.1
	$_{NCL}$N-H···OH$_{NCL}$	13.7	12.7	1.739	137.6
	$_{IMI}$N-H···O$_{ket}$	11.7	12.7	2.223	132.7
NCL-MeOH	$_{NCL}$O-H···OH	13.1	12.3	1.526	173.2
	$_{NCL}$N-H···OH$_{NCL}$	11.9	11.7	1.724	139.7
NCL-CAF	$_{NCL}$O-H···O	10.8	10.5	1.661	177.6
	$_{NCL}$N-H···OH$_{NCL}$	11.4	11.0	1.774	139.3
NCL-URE	$_{NCL}$O-H···O	12.5	12.2	1.599	177.3
	$_{NCL}$N-H···OH$_{NCL}$	10.5	9.8	1.792	138.5

Co-crystallization of molecular solids typically entails rearrangement of the hydrogen bonding network thus rendering the involved protons, the donor/acceptor atoms and their neighboring atoms sufficiently sensitive solid state NMR probes for the validation of proposed structure models. The experimental MAS NMR and DFT computed ^{1}H chemical shifts of the important hydrogen bonds that stabilize the resulting crystal packing within the considered crystal structures are summarized in Table 2, and in all cases fit well within ±1 ppm, including NCL-AA-I and NCL-AA-II. In some cases, however, even upon inspection

of the corresponding ^{1}H-^{1}H DQMAS NMR spectra, the experimental ^{1}H chemical shifts could not be unambiguously resolved, and thus were excluded from validation.

Table 3: *Experimental and calculated ^{13}C chemical shifts of NCL hydrate H_A and selected co-crystals.*

Phase	**δ_{iso} ^{13}C(C-OH) exp., (DFT) /ppm**	**δ_{iso} ^{13}C(C=O) exp., (DFT) /ppm**	**δ_{iso} ^{13}C(C_{amide}) exp., (DFT) /ppm**	**δ_{iso} ^{13}C(C-N-C) exp., (DFT) /ppm**
NCL	154.0	163.0		
NCL-H_A	154.7, (156.7)	162.8, (160.3)		
NCL-AA-I	155.4, (159.9)	163.3, (165.4)	178.7 (171.6)	
NCL-AA-II	154.1, (156.4)	161.8, (170.5)	179.9 (171.5)	
NCL-BA	156.1	164.8	173.5	
NCL-IN	155.4	163.9	151.9	150.2/148.2
NCL-NA	155.9	164.7	169.4	148.0/149.0
NCL-IA	156.3	162.8	166.1	150.2/150.2
NCL-AT	157.6, (158.1)	165.9, (165.0)	172.3 (172.3)	134.9, (134.2)
NCL-IMI	166.3, (172.3)	161.6, (167.6)		143.0, (137.0)

In addition, the experimental and DFT computed ^{13}C chemical shifts of selected co-crystals are collected in Table 3. While in most cases, the calculated shifts fit reasonably well (± 6 ppm) with the experimental values, the deviation is somewhat larger in case of NCL-AA-I and NCL-AA-II, though the agreement is much better than in case of those structure solutions considered as not validated. Nevertheless, since the agreement is good for the ^{1}H NMR shifts which are considered to be more reliable probes for the evaluation of structures,[133-135] the obtained structure solutions for NCL-H_A (in agreement with a recently reported structure[38]), NCL-AT, NCL-AA-I, NCL-AA-II, and NCL-IMI could be successfully validated. Note that the ^{15}N NMR chemical shifts are not well reproduced at the applied level of theory, rather reflecting trends, and thus are not included in the structure validation. Since both the ^{1}H and ^{13}C DFT computed chemical shifts of structure solutions derived for the co-compounds NCL-BA, NCL-IN, NCL-NA and NCL-IA were inconsistent with the available experimental solid state NMR data, these structures could not be validated even though they exhibited plausible hydrogen bonding pattern as well as reasonably good profile fits and *R*-values.

Thermal Stability of Niclosamide Co-crystals. The thermal stability and phase transition of drugs or active pharmaceutical ingredients are highly important to elucidate physicochemical and/or pharmacokinetic properties and likely changes thereof upon prolonged storage due to e.g. de-/rehydration or polymorphism, respectively. The DSC curve obtained for NCL-AA-II

indicated two endotherm peaks at 171.5°C and 157.7°C (which could be due to the presence of residual NCL-AA-I), followed by the sublimation of AA and melting process of pristine NCL. In contrast, the polymorph NCL-AA-I showed merely one endotherm peak at 159.2°C in addition to sublimation of AA and melting of NCL even though the multiphase Rietveld analysis indicated a larger residual fraction of NCL-AA-II. Note that the dehydration of NCL-H_A was observed at 86.9°C while the remaining new co-crystals exhibited a single endotherm peak at temperatures ranging between those of the pristine drug and co-formers thereby suggesting no decomposition before melting (Table 4).

Table 4: *Melting points and endotherm peaks identified in the corresponding DSC curves of NCL co-crystals and NCL-H_A hydrate. In case of NCL-AA-II, the peak marked with an asterisk could be due to residual NCL-AA-I; in case of NCL-NA, the melting point is not well-defined.*

Phase	**Peak /°C**
NCL	228.3
NCL-H_A	86.9 (dehydration)
NCL-AA-I	159.2
NCL-AA-II	157.7*; 171.5
NCL-BA	189.6
NCL-IN	185.5
NCL-NA	≈222.7
NCL-IA	226.7
NCL-AT	187.5
NCL-IMI	213.5

Table 5: *The determined equilibrium solubility of the considered NCL co-crystals. Reference data obtained from already reported co-crystals[48] is given in brackets for comparison. Note that the discrepancies likely result from normalization with respect to a fixed amount of NCL per sample.*

Phase	***Solubility at 37° C (24 h) in 40% isopropanol-water mixture (mg L^{-1})***
NCL	87.15
NCL-AA-I	122.29 (x1.4)
NCL-BA	109.34 (x1.3)
NCL-IN	105.29 (x1.2)
NCL-NA	114.45 (x1.3) [x1.2][48]
NCL-IA	113.45 (x1.3) [x1.7][48]
NCL-AT	**245.87 (x2.8)**
NCL-URE	84.89 (x1.0) [x2.0][48]
NCL-CAF	114.5 (x1.3) [x1.3][48]
NCL-PABA	109.1 (x1.1) [x0.8][48]

Solubility of Niclosamide Co-crystals. The equilibrium solubility of NCL, the obtained co-crystals and some reference compounds was determined based on reported procedures,[136,137]

and could be reproduced in repeated measurements (Table 5). Since co-crystals containing low molecular weight co-formers may exhibit superior solubility compared to other formulations, we have normalized the amount of NCL actually present in the tested compounds to 50 mg per sample, thereby adjusting the initially weighted sample accordingly, in this way allowing better comparability of the determined solubility values (note that NCL-AA-II and NCL-IMI were both excluded from the solubility tests). Nevertheless, the solubility values of NCL-NA, NCL-IA, NCL-URE and NCL-PABA co-crystals derived from our measurements differ from the reported data, likely resulting from the fact that in reference [48] the authors did not normalize the weights of solid material used for solubility tests to the actual amount of NCL. Among the considered compounds, the most significant solubility improvement could be achieved in case of NCL-AT whose equilibrium solubility was found to be 2.8 times higher than that of pristine NCL, which (to the best of our knowledge) is the highest equilibrium solubility of NCL co-crystals currently observed. Rather unexpectedly, the reasonably high solubility of NCL-URE reported in the literature could not be reproduced, possibly due to undesired hydrate formation upon prolonged storage (a strong tendency for hydrate formation has previously been observed for NCL-PABA, NCL-URE and NCL-CAF after a storage period of 4–6 weeks).[48] In contrast, the novel NCL-AT co-crystal is demonstrably stable for a period of more than 18 months, most probably due to its strong hydrogen bonding motifs. Also, a moderately increased equilibrium solubility was observed for the co-crystals of NCL-BA, NCL-IN and NCL-AA-I, respectively.

3. Conclusion

An enhanced equilibrium solubility of the anthelmintic drug *niclosamide* could be achieved via hydrogen bond mediated co-crystal formation based on crystal engineering principles. Suitable co-formers of NCL were taken from the GRAS and EAFUS lists, thereby rendering all obtained co-phases not involving salt formation pharmaceutically acceptable and promising candidates for the current trend of repurposing long known drugs for the treatment of lifestyle diseases such as cancer.[138] Aspects of "green chemistry" were also considered by producing the new crystalline phases from either solvent-drop assisted grinding and/or mechanical treatment in addition to slow evaporation from environmentally friendly solvents such as ethanol. Indeed, structure solutions for NCL-AT, NCL-IMI, the polymorphs NCL-AA-I and NCL-AA-II, and NCL-H_A[38] were derived from powdered samples combining powder X-ray diffraction and solid state NMR data, evidencing successful co-crystal

formation based on the rather robust {O–H···O}, {N–H···O} and {O–H···N} synthons, respectively.

4. Experimental Section

NCL was purchased from Cayman Chemical Company (Tallinn, Estonia) while AA, AT, BA and NA were obtained from Acros Organics (Geel, Belgium); IA and IN were delivered from Sigma Aldrich (Saint-Quentin Fallavier, France). All compounds were used without further purification.

Synthesis. *Niclosamide hydrate, NCL-H_A.* 100 mg (0.31 mmol) of niclosamide were refluxed in water (6 mL) for 2 h and the product was cooled to room temperature over 6 h. Dehydration 86.9 °C.

NCL-IMI (1:1) Co-crystal. 500 mg (1.53 mmol) of niclosamide and 104.06 mg (1.53 mmol) of imidazol were ground in mortar-pestle for 15 min after adding 5 drops of dry EtOH. Mp 213.5 °C.

NCL-AT (1:1) Co-crystal. 460 mg (1.41 mmol) of niclosamide and 140.82 mg (1.41 mmol) of 2-aminothiazole were ground in mortar-pestle for 15 min after adding 5 drops of dry EtOH. Mp 187-189 °C.

NCL-AA-I (1:1) Co-crystal. 510 mg (1.56 mmol) of niclosamide and 92.09 mg (1.56 mmol) of acetamide were ground in mortar-pestle for 15 min after adding 5 drops of dry EtOH. Mp 158-160 °C.

NCL-AA-II (1:1) Co-crystal. 510 mg (1.56 mmol) of niclosamide and 92.09 mg (1.56 mmol) of acetamide were ground in mortar-pestle for 15 min after adding 5 drops of Acetone. Mp 157-159 °C.

NCL-BA (1:1) Co-crystal. 450 mg (1.38 mmol) of niclosamide and 166.65 mg (1.38 mmol) of benzamide were ground in mortar-pestle for 15 min after adding 5 drops of dry EtOH. Mp 189-191 °C.

NCL-IN (1:1) Co-crystal. 430 mg (1.31 mmol) of niclosamide and 180.27 mg (1.31 mmol) of isoniazide were ground in mortar-pestle for 15 min after adding 5 drops of dry EtOH. Mp 185-187 °C.

NCL-NA (1:1) Co-crystal. 450 mg (1.38 mmol) of niclosamide and 167.99 mg (1.38 mmol) of nicotinamide were ground in mortar-pestle for 15 min after adding 5 drops of dry EtOH. Mp 221-223 °C.

NCL-IA (1:1) Co-crystal. 450 mg (1.38 mmol) of niclosamide and 167.99 mg (1.38 mmol) of isonicotinamide were ground in mortar-pestle for 15 min after adding 5 drops of dry EtOH. Mp 226–228 °C.

Powder X-ray Diffraction. Bulk samples for phase identification were analyzed by PXRD on a Bruker D8 Discover powder diffractometer. Experimental conditions: Cu–K$\alpha_{1/2}$ radiation (λ_1 = 1.540596 Å, λ_2 = 1.544410 Å; ratio $K\alpha_1/ K\alpha_2$ = 0.441122); 40 kV; 40 mA; scanning interval 5–50° 2θ at a step size of 0.01°; time per step 3 s; T = 295 K in Bragg-Brentano geometry. In addition, all samples for structure solution were analyzed with a STOE StadiP powder diffractometer. Experimental conditions: Cu–Kα_1 radiation (λ_1 = 1.540598 Å); 45 kV; 30 mA; scanning interval 0–70° 2θ at a step size of 0.1°; time per step 120 s; T = 293 K in Debye-Scherrer geometry. Indexing of the powder patterns was performed using *N-TREOR*[139] and further confirmed with *DICVOL04*.[140] The corresponding cell volume was verified by calculating expected cell volumes from volume increments. [141] For space group determination Le-Bail refinement was used for whole pattern fitting thereby extracting the integrated peak intensities and their correlations using the *expo2014* software package. Structures were solved in direct space using the *simulated annealing* (SA) approach or *hybrid big bang big crunch* (HBB-BC) algorithm as implemented in *expo2014*, allowing flexible torsion angles as well as six degrees of freedom for rotation and translation, respectively, for each molecule. After an initial structure model was obtained with all hydrogen atoms removed during the optimization (50 runs) hydrogen atoms were inserted at typical positions using *Mercury 3.3* and Rietveld refinement was then performed using Bruker *TOPAS 4.2*.

Solid-State NMR spectroscopy. Solid-state NMR measurements were performed on either BRUKER AVANCE III 300 or AVANCE DSX 500 spectrometers, corresponding to magnetic flux densities of 7.05 T and 11.74 T. The spectrometers were equipped with commercially available BRUKER 4 mm double and triple resonance probes operating at MAS rotation frequencies between 3.0 and 15.0 kHz while at the 500 MHz spectrometer, either 2.5 mm triple or double resonance probes operating at MAS rotation frequencies of up to 30 kHz were applied. $^{13}C\{^{1}H\}$ cross-polarization (CP)-MAS NMR spectra were measured with ^{1}H 90° pulse lengths of 5 μs (corresponding to a radiofrequency field (ν_1) of 50 kHz), a contact time of 2.5 ms with spinning frequency of 12 kHz and relaxation delays of 10 to 120 s, depending on the proton T_1 relaxation times. Hartmann – Hahn conditions were adjusted on 1-^{13}C-^{15}N-labelled α-glycine; an efficient polarization transfer was achieved by a ramped-amplitude CP step with $\nu_1(^{1}H)$ being swept from 54 kHz to 27 kHz in 64 steps (in the case of a ^{1}H 90° pulse length of 5.0 μs).[142] All the spectra were obtained with TPPM-15 proton decoupling[143] during the data acquisition applying decoupling pulses of 6.7 μs to 10.0 μs length (~10/12 π-pulse). Chemical shifts are reported relative to the secondary standard 1-^{13}C-^{15}N-labelled glycine (1-^{13}C signal at 176.5 ppm). The $^{15}N\{^{1}H\}$ CPMAS-NMR experiments were performed at 7.05 T using the following acquisition parameters: a ^{1}H 90° pulse length of 7.0 μs, a contact time of 5 ms, a spinning speed of 10 kHz and a relaxation delay of 10-30 s; ^{15}N chemical shifts are reported with respect to 1-^{13}C-^{15}N-labelled glycine (set to -347.6 ppm). All the ^{1}H MAS NMR spectra were measured at 11.74 T with 2.5 μs 90° pulse length, a spinning speed of 30 kHz, and relaxation delays of 120-2000 s. A back-to-back (BaBa) recoupling sequence was used to excite and reconvert double-quantum (DQ) coherences at 11.74 T with 2.5 μs 90° pulse length, a spinning speed of 29762 Hz (due to rotor-synchronized detection in the F1 dimension), a dwell time of 5 μs and an excitation time of τ_{exc}=33.6 μs. For the 2D ^{1}H-^{1}H DQ-MAS-NMR experiments 64-256 t_1 increments in steps of 33.6 μs (corresponding to a rotor period) and 16 transients per increment were acquired. Spectral deconvolution and line-shape analysis were performed with DMFIT (version 2011).[144]

Thermal Analysis. DSC analysis of the co-phases was performed on a NETZSCH DSC 204 Phoenix®. Samples were placed in crimped but vented aluminum pans. A typical sample size was 4 – 10 mg, the measured temperature range was {20 – 250°C} at 10 °C/min; all samples were purged with a dry nitrogen flow at 125 mL/min during the measurement.

Solubility Experiments. The quantification of NCL was validated using a Phenomenex Gemini-NX HPLC-UV/vis and a C18 column (250 mm x 4.6 mm, 5 mm particle diameter). The mobile phase consisted of a 0.05 M methanol / $(NH_4)_3PO_4$ (9:1) buffer, adjusted to a pH value of 3.6 with H_3PO_4. The considered concentration range of NCL was in between 0.5-100 µg/mL. The flow rate and the injection volume was set to 1.0 mL/min and 50 µL, respectively. The limit of detection was 0.1 µg/mL and the limit of quantification 0.5 µg/mL. The absorbance was measured at 254 nm. The equilibrium solubility was determined in 40%-isopropanol – water medium using the shake-flask method.[136,137] Accordingly, each solid sample containing 50 mg of NCL was stirred for 24 h at 37°C in 2.5 mL of the medium. The concentration of the saturated solution was calculated after 24 h which is referred to as the equilibrium solubility of the considered solid form.

DFT calculations. For the sake of reasonable accuracy at affordable computational costs, the DFT chemical shift calculations were performed in Gaussian09[145] considering suitably chosen cluster models that were extracted from the obtained PXRD structure solutions or where available from single-crystal data. The cluster models were created such that all characteristic hydrogen bonds or close proximities due to packing were satisfied. Though the hydrogen atoms were Rietveld refined in the final step of the structure solution process, all atoms except for hydrogen were "frozen" at given coordinates (assuming that a reasonable "skeleton" structure was derived from Rietveld refinement) for H-bond length optimization (opt = ModRedundant) at DFT/PBE1PBE/6-311G(d,p) level of theory. The ^{1}H and ^{13}C chemical shielding values were computed from optimized cluster models (considering important hydrogen bonding, short contacts and molecular packing) at PBE1PBE/6-311G(d,p) level of theory and "translated" into the corresponding chemical shifts with respect to either benzene (^{1}H, ^{13}C) or methanol (^{1}H, ^{13}C), respectively, depending on the orbital hybridization: sp3 (methanol); sp2,sp (benzene)) following the multi-standard approach.[131,132]

Supporting Information Available: $^{13}C\{^{1}H\}$ & $^{15}N\{^{1}H\}$ CPMAS and 2D ^{1}H–^{1}H DQMAS NMR spectra (except for NCL-IMI) as well as additional PXRD data of the co-crystals are available free of charge via internet at http://pubs.acs.org. The following crystal structures have been submitted to the Cambridge Crystallographic Data Centre (CCDC): NCL-AT (1437254), NCL-AA-II (1437255), NCL-AA-I (1437256), NCL-HA (1437257), NCL-IMI_salt (1437258).

Notes: Some parts of the publication required for patent application were submitted to the European Patent Office (application number EP15193955.0).

Acknowledgements

Funding by the Deutsche Forschungsgemeinschaft (DFG) project EC168/10-2 ("Dynamische Supramolekulare Assoziationen") is gratefully acknowledged. G. B. appreciates access to the High Performance Computing facilities (WWU-PALMA), kindly provided by Prof. A. Heuer (Univ. Münster). Prof. M. Winter (Univ. Münster, MEET) is acknowledged for his support and for providing access to Bruker D8 powder X-ray diffractometers. In addition, technical support and maintenance of the STOE StadiP powder diffractometer by T. Fickenscher (Univ. Münster) is highly appreciated.

5. References

(1) Craig, P.; Akira, I. *Curr. Opin. Infect. Dis.* **2007**, *20*, 524.

(2) Scholefield, R. J.; Bergstedt, R. A.; Bills, T. D. *J. Great Lakes Res.* **2003**, *29*, 493.

(3) Huang, H. C.; Liao, S. C.; Chang, F. R.; Kuo, Y. H.; Wu, Y. C. *J. Agr. Food Chem.* **2003**, *51*, 4916.

(4) Park, S. J.; Shin, J. H.; Kang, H.; Hwang, J. J.; Cho, D. H. *BMB Rep.* **2011**, *44*, 517.

(5) Abreu, F. C.; Goulart, M. O. F.; Oliveira, A. B. M. *Biosens. Bioelectron.* **2002**, *17*, 913.

(6) Lardans, V.; Dissous, C. *Parasitol. Today* **1998**, *14*, 413.

(7) Andrews, P.; Thyssen, J.; Lorke, D. *Pharmacol. Therapeut.* **1983**, *19*, 245.

(8) Gill, G.; Beeching, N. *Lecture Notes: Tropical Medicine* **2009**, 6th edition, Blackwell Publishing Ltd., pp. 202 – 207.

(9) World Health Organization: Specification and Evaluation for Public Health Pesticides (Niclosamide). Geneva: WHO **2002**, 1.

(10) Chang, Y. W.; Yeh, T. K.; Lin, K. T.; Chen, W. C.; Yao, H. T.; Lan, S. J.; Wu, Y. S.; Hsieh, H. P.; Chen, C. M.; Chen, C. T. *J. Food Drug Anal.* **2006**, *14*, 329.

(11) Al-Hayida, B. M. *Profiles Drug Subst. Excip. Relat. Methodol.* **2005**, *32*, 67.

(12) Liang, L.; Huang, M.; Xiao, Y.; Zen, S.; Lao, M.; Zou, Y.; Shi, M.; Yang, X.; Xu, H. *Inflamm. Res.* **2015**, *64*, 225.

(13) Gies, E.; Wilde, I.; Winget, J. M.; Brack, M.; Rotblat, B.; Novoa, C. A.; Balgi, A. D.; Sorensen, P. H.; Roberge, M.; Mayor, T. *PLOS One* **2010**, *5*, e14410.

(14) Li, Y.; Li, P. K.; Roberts, M. J.; Arend, R. C.; Samant, R. S.; Buchsbaum, D. J. *Cancer Lett.* **2014**, *349*, 8.

(15) Lee, S.; Son, A. R.; Ahn, J.; Song, Y. J. *Biomed. Pharmacother.* **2014**, *68*, 619.

(16) Yokoama, M. *J. Drug Target.* **2014**, *22*, 576.

(17) Crucho, C. I. C. *ChemMedChem* **2015**, *10*, 24.

(18) Dong, R.; Zhou, Y.; Huang, X.; Zhu, X.; Lu, Y.; Shen, J. *Adv. Mater.* **2015**, *27*, 498.

(19) Ma, X.; Zhao, Y. *Chem. Rev.* **2015**, *115*, 7794.

(20) Zhang, M.; Xuzhou, H.; Feihe, N.; Gibson, H. W. *Acc. Chem. Res.* **2014**, *47*, 1995.

(21) Ghosh, I.; Nau, W. M. *Adv. Drug. Delivery Rev.* **2012**, *64*, 764.

(22) Morissette, S. L.; Almarsson, Ö.; Petersson, M. L.; Remenar, J. F.; Read, M. J.; Lemmo, A. V.; Ellis, S.; Cima, M. C.; Gardner, C. R. *Adv. Drug Delivery Rev.* **2004**, *56*, 275.

(23) Huang, L. F.; Tong, W. Q. *Adv. Drug Delivery Rev.* **2004**, *56*, 321.

(24) Storey, R.; Docherty, R.; Higginson, P.; Dallman, C.; Gilmore, C.; Barr, G.; Dong, W. *Crystallography Reports* **2004**, *10*, 45.

(25) Yu, L. *Adv. Drug Delivery Rev.* **2001**, *48*, 27.

(26) Laitinen, R.; Löbmann, K.; Strachan, C. J.; Grohganz, H.; Rades, T. *Int. J. Pharm.* **2013**, *453*, 65.

(27) Kaushal, A. M.; Gupta, P.; Bansal, A. K. *Crit. Rev. Ther. Drug Carrier Syst.* **2004**, *21*, 133.

(28) Craig, D. Q. M.; Royal, P. G.; Kett, V. L.; Hopton, M. L. *Int. J. Pharm.* **1999**, *179*, 179.

(29) Löbmann, K.; Laitinen, R.; Grohganz, H.; Gordon, K. C.; Strachan, C.; Rades, T. *Mol. Pharmaceutics* **2011**, *8*, 1919.

(30) Alhalaweh, A.; Alzghoul, A.; Kaialy, W.; Mahlin, D.; Bergström, C. A. S. *Mol. Pharmaceutics* **2014**, *11*, 3123.

(31) Dai, J.; Wang, W.; Liang, Y.; Li, H.; Guan, X.; Zhu, Y. *Parasitol. Res.* **2008**, *103*, 405.

(32) Kenawy, E.; Rizk, E. *Macromol. Biosci. Polymer* **2004**, *4*, 119.

(33) Yang, W.; de Villiers, M. M. *AAPS J.* **2005**, *7*, E241.

(34) Devarakonda, B.; Hill, R. A.; Liebenberg, W.; Brits, M.; de Villiers, M. M. *Int. J. Pharm.* **2005**, *304*, 193.

(35) Bai, M. Y.; Yang, H. C. *Colloids and Surfaces A: Physicochem. Eng. Aspects* **2012**, *419*, 248.

(36) Jin, Y.; Lu, Z.; Ding, K.; Li, J.; Du, X.; Chen, C.; Sun, X.; Wu, Y.; Zhou, J.; Pan, J. *Cancer Res.* **2010**, *70*, 2516.

(37) Chen, H.; Yang, Z.; Ding, C.; Chu, L.; Zhang, Y.; Terry, K.; Liu, H.; Shen, Q.; Zhou, J. *ACS Med. Chem. Lett.* **2013**, *4*, 180.

(38) Sovago, I.; Bond, A. D. *Acta. Cryst. C* **2015**, *71*, 394.

(39) Gallardo-Godoy, A.; Gever, J.; Fife, K. L.; Silber, B. M.; Prusiner, S. B.; Renslo, A. R. *J. Med. Chem.* **2011**, *54*, 1010.

(40) Steed, J. W. *Trends Pharmacol. Sci.* **2013**, *34*, 185.

(41) Miroshnyk, I.; Mirza, S.; Sandler, N. *Expert Opin. Drug Delivery* **2009**, *6*, 333.

(42) Aakeröy, C. B.; Forbes, S.; Desper, J. *CrystEngComm* **2014**, *16*, 5870.

(43) Khan, M.; Enkelmann, V.; Brunklaus, G. *J. Am. Chem. Soc.* **2010**, *132*, 5254.

(44) Springuel, G.; Norberg, B.; Robeyns, K.; Woutes, J.; Leyssens, T. *Cryst. Growth Des.* **2012**, *12*, 475; Stanton, M. K.; Tufekcic, S.; Morgan, C.; Bak, A. *Cryst. Growth Des.* **2008**, *9*, 1344.

(45) Khan, M.; Enkelmann, V.; Brunklaus, G. *CrystEngComm* **2011**, *13*, 3213.

(46) Thakuria, R.; Delori, A.; Jones, W.; Lipert, M. P.; Roy, L.; Rodriguez-Hornedo, N. *Int. J. Pharm.* **2013**, *453*, 101.

(47) Trask, A. V. *Mol. Pharm.* **2007**, *4*, 301.

(48) Sanphui, P.; Kumar, S. S.; Nangia, A. *Cyrst. Growth Des.* **2012**, *12*, 4588.

(49) Merz, K.; Vasylyeva, V. *CyrstEngComm* **2010**, *12*, 3989.

(50) Desiraju, G. R. *Angew. Chem. Int. Ed.* **1995**, *34*, 2311.

(51) Desiraju, G. R. *Chem. Commun.* **1997**, *16*, 1475.

(52) Khan, M.; Enkelmann, V.; Brunklaus, G. *J. Org. Chem.* **2009**, *74*, 2261.

(53) Khan, M.; Enkelmann, V.; Brunklaus, G. *CrystEngComm* **2009**, *74*, 1001.

(54) Khan, M.; Enkelmann, V.; Brunklaus, G. *Cryst. Growth Des.* **2009**, *9*, 2354.

(55) Grifasi, F.; Chierotti, M. R.; Gaglioti, K.; Gobetto, R.; Maini, L.; Braga, D.; Dichiarante, E.; Curzi, M. *Cryst. Growth Des.* **2015**, 15, 1939.

(56) Hanslick, J. L.; Lau, K.; Noguchi, K. K., Olney, J. W.; Zorumski, C. F.; Mennerick, S.; Farber, N. B. *Neurobiol. Dis.* **2009**, *34*, 1.

(57) Luedeker, D.; Brunklaus, G. *Solid State Nucl. Magn. Reson.* **2015**, *65*, 29.

(58) Harris, R. K.; Wasylishen, R. E.; Duer, M. J. *NMR Crystallography*, Wiley, **2009**.

(59) Taulelle, F. *Solid State Sci.* **2004**, *6*, 1053.

(60) Senker, J.; Seyfarth, L.; Voll, J. *Solid State Sci.* **2004**, *6*, 1029.

(61) Harris, R. K. *Solid State Sci.* **2004**, *6*, 1025.

(62) Ashbrook, S. E. *Phys. Chem. Chem. Phys.* **2009**, *11*, 6892.

(63) Ashbrook, S. E.; Duer, M. J. *Concepts Magn. Reson. A* **2006**, *28*, 183.

(64) Harris, R. K.; Hodgkinson, P.; Pickard, C. J.; Yates, J. R.; Zorin, V. *Magn. Reson. Chem.* **2007**, *45*, S174.

(65) Harris, K. D. M. *Top. Curr. Chem.* **2012**, *315*, 133.

(66) Powell, H. R. *Annu. Rep. Prog. Chem. C* **2010**, *106*, 192.

(67) Price, S. L. *Acc. Chem. Res.* **2009**, *42*, 117.

(68) Lehmann, C. W. *Angew. Chem. Int. Ed.* **2011**, *50*, 5616.

(69) Day, G. M. *Crystallogr. Rev.* **2011**, *17*, 3.

(70) Apperley, D. C.; Bastanov, A. S.; Clark, S. J.; Harris, R. K.; Hodgkinson, P. Jochym, D. B. *J. Mol. Struct.* **2012**, *1015*, 192.

(71) Filip, X.; Borodi, G.; Filip, C. *Phys. Chem. Chem. Phys.* **2011**, *13*, 17978.

(72) Webber, A. L.; Emsley, L.; Clarmunt, R. M.; Brown, S. P. *J. Chem. Phys. A* **2010**, *114*, 10435.

(73) Tishmack, P. A.; Bugay, D. E.; Byrn, S. R. *J. Pharm. Sci.* **2003**, *92*, 441.

(74) Dudenko, D.; Williams, P. A.; Hughes, C. E.; Antzutkin, O. N.; Velaga, S. P.; Brown, S. P.; Harris, K. D. M. *J. Chem. Phys. C.* **2013**, *117*, 12258.

(75) Tatton, A. S.; Pham, T. M.; Vogt, F. G.; Iuga, D.; Edwards, A. J.; Brown, S. P. *CrystEngComm* **2012**, *14*, 2654.

(76) Harper, J. K.; Grant, D. M. *Cryst. Growth Des.* **2006**, *6*, 2315.

(77) Martineau, C.; Senker, J.; Taulelle, F. *Annu. Rep. NMR Spectrosc.* **2014**, *82*, 1.

(78) Reddy, G. N. M.; Cook, D. S.; Iuga, D.; Walton, R. I.; Marsh, A.; Brown, S. P. *Solid State Nucl. Magn. Reson.* **2015**, *65*, 41.

(79) Martineau, C.; Vial, S.; Barth, D.; Quessette, F.; Taulelle, F. *Solid State Nucl. Magn. Reson.* **2015**, *65*, 84.

(80) Brouwer, D. H.; Horvath, M. *Solid State Nucl. Magn. Reson.* **2015**, *65*, 89.

(81) Filip, X.; Filip, C. *Solid State Nucl. Magn. Reson.* **2015**, *65*, 21.

(82) Zehe, C. S.; Siegel, R.; Senker, J. *Solid State Nucl. Magn. Reson.* **2015**, *65*, 122.

(83) Paluch, P.; Pawlak, T.; Oszajca, M.; Lasocha, W.; Potrzebowski, M. J. *Solid State Nucl. Magn. Reson.* **2015**, *65*, 2.

(84) Berzins, A.; Hodgkinson, P. *Solid State Nucl. Magn. Reson.* **2015**, *65*, 12.

(85) Mollica, G.; Dekhil, M.; Ziarelli, F.; Thureau, P.; Viel, S. *Solid State Nucl. Magn. Reson.* **2015**, *65*, 114.

(86) Sardo, M.; Santos, S. M.; Babaryk, A. A.; Lopez, C.; Alkorta, I.; Elguero, J.; Claramunt, R. M.; Mafra, L. *Solid State Nucl. Magn. Reson.* **2015**, *65*, 49.

(87) Elena, B.; Emsley, L. *J. Am. Chem. Soc.* **2005**, *127*, 9140.

(88) Santos, S. M.; Rocha, J.; Mafra, L. *Cryst. Growth Des.* **2013**, *13*, 2390.

(89) Lorente, P.; Shenderovich, I. G.; Golubev, N. S.; Denisov, G. S.; Buntkowsky, G.; Limbach, H. H. *Magn. Reson. Chem.* **2001**, *39*, S18.

(90) Xu, X.; Kanzaki, M. *J. Am. Ceram. Soc.* **2009**, *92*, 2803.

(91) Ip, B. C. K.; Shenderovich, I. G.; Tolstoy, P. M.; Frydel, J.; Denisov, G. S.; Buntkowsky, G.; Limbach, H. H. *J. Phys. Chem. A* **2012**, *116*, 11370.

(92) Shenderovich, I. G.; Buntkowsky, G.; Schreiber, A.; Gedat, E.; Sharif, S.; Albrecht, J.; Golubev, N. S.; Findenegg, G. H.; Limbach, H. H. *J. Phys. Chem. B* **2003**, *107*, 11924.

(93) Kalakewich, K.; Iuliucci, R.; Harper, J. K. *Cryst. Growth Des.* **2013**, *13*, 5391.

(94) Suzuki, F.; Fukushima, T.; Fuckuchi, M.; Kaji, H. *J. Phys. Chem. C* **2013**, *117*, 18809.

(95) Filip, X.; Grosu, I. G.; Miclaus, M.; Filip, C. *CrystEngComm* **2013**, *15*, 4131.

(96) Nather, C.; Jess, I.; Seyfarth, L.; Barwinkel, K.; Senker, J. *Cryst. Growth Des.* **2015**, *15*, 366.

(97) Marker, K.; Pingret, M.; Mouesca, J. M.; Gasparutto, D.; Hediger, S.; De Paepe, G. *J. Am. Chem. Soc.* **2015**, *137*, 13796.

(98) Mafra, L.; Santos, S. M.; Siegel, R.; Alves, I.; Almeida Paz, F. A.; Dudenko, D.; Spiess, H. W. *J. Am. Chem. Soc.* **2011**, *134*, 71.

(99) Salager, E.; Stein, R. S.; Pickard, C. J.; Elena, B.; Emsley, L. *Phys. Chem. Chem. Phys.* **2009**, *11*, 2610.

(100) Miclaus, M.; Grosu, I. G.; Filip, X.; Tripon, C.; Filip, C. *CrystEngComm* **2014**, *16*, 299.
(101) Macholl, S.; Tietze, D.; Buntkowsky, G. *CrystEngComm* **2013**, *15*, 8627.

(102) Mueller, L. J.; Dunn, M. F. *Acc. Chem. Res.* **2013**, *46*, 2008.

(103) Taulelle, F.; Bouchevreau, B.; Martineau, C. *CrystEngComm* **2013**, *15*, 8613.

(104) Bhaumik, A.; Luchinat, C.; Parigi, G.; Ravera, E.; Rinaldelli, M. *CrystEngComm* **2013**, *15*, 8639.

(105) Koller, H.; Weiss, M. *Top. Curr. Chem.* **2012**, *306*, 189.

(106) Brouwer, D. H.; Alavi, S.; Ripmeester, J. A. *Phys. Chem. Chem. Phys.* **2008**, *10*, 3857.

(107) Wiegand, T.; Luedeker, D.; Brunklaus, G.; Bussmann, K.; Kehr, G.; Erker, G.; Eckert, H. *Dalton Trans.* **2014**, *43*, 12639.

(108) Schmidt, M.; Zehe, C. S.; Siegel, R.; Heigl, J. U.; Steinlein, C.; Schmidt, H. W.; Senker, J. *CrystEngComm* **2013**, *43*, 8784.

(109) Fonseca, I.; Baias, M.; Hayes, S. E.; Pickard, C. J.; Bertmer, M. *J. Chem. Phys. C* **2012**, *116*, 12212.

(110) Schultheiss, N.; Newman, A. *Cryst. Growth Des.* **2009**, *9*, 2950.

(111) Harriss, B. I.; Wilson, C.; Evans, I. R. *Acta Cryst. C* **2014**, *70*, 758.

(112) van Tonder, E. C.; Mahlatji, M. D.; Malan, S. F.; Liebenberg, W.; Caira, M. R.; Song, M.; de Villiers, M. M. *AAPS Pharm. Sci. Tech.* **2004**, *5*, 1.

(113) Caira, M. R.; van Tonder, E. C.; de Villiers, M. M.; Lötter, A. P. *J. Inclusion Phenom. Mol. Recognition Chem.* **1998**, *31*, 1.

(114) van Tonder, E. C.; Maleka, . T. S. P.; Liebenberg, W.; Song, M. N.; Wurster, D. E.; de Villeiers, M. M. *Int. J. Pharm.* **2004**, 269, 417.

(115) Tian, F.; Qu, H.; Louhi-Kultanen, M.; Ratanen, J. *Chem. Eng. Technol.* **2010**, *33*, 833.

(116) Khankari, R. K.; Grant, D. J. W. *Thermochim. Acta* **1995**, *248*, 61.

(117) van de Streek, J.; Motherwell, S. *CrystEngComm* **2007**, *9*, 55.

(118) Steiner, T. *Angew. Chem. Int. Ed.* **2002**, *41*, 48.

(119) Aliev, A. E.; Harris, K. D. M. *Struct. Bond.* **2004**, *108*, 1.

(120) Chierotti, M. R.; Gobetto, R. *Chem. Commun.* **2008**, 1621.

(121) Harris, R. K.; Ghi, P. Y.; Hammond, R. B.; Ma, C. Y.; Roberts, K. J. *Chem. Commun.* **2003**, 2834.

(122) Bolz, I.; Moon, C.; Enkelmann, V., Brunklaus, G.; Spange, S. *J. Org. Chem.* **2008**, *73*, 4783.

(123) Brown, S. P.; Spiess, H. W. *Chem. Rev.* **2001**, *101*, 4125.

(124) Brown, S. P. *Prog. Nucl. Magn. Reson.* **2007**, *50*, 199.
(125) Bradley, J. P.; Velaga, S. P.; Antzutkin, D.N. Brown, S. P. *Cryst. Growth Des.* **2011**, *11*, 3463.

(126) Bradley, J. P.; Pickard, C. J.; Burley, J. C.; Martin, D. R.; Hughes, L. P.; Cosgrove, S. D.; Brown, S. P. *J. Pharm. Sci.* **2012**, *101*, 1821.

(127) Khan, M.; Enkelmann, V.; Brunklaus, G. *J. Org. Chem.* **2009**, *74*, 2261.

(128) Krushelnitsky, A.; Kurbanov, R.; Reichert, D.; Hempel, G.; Schneider, H.; Fedotov, V. *Solid State Nucl. Magn. Reson.* **2002**, *22*, 423.

(129) Gorelik, T. E.; van de Streek, J.; Kilbinger, A. F. M.; Brunklaus, G.; Kolb, U. *Acta Cryst.* **2012**, *B68*, 171.

(130) Johnston, J. C.; Iuliucci, R. J.; Facelli, J. C.; Fitzgerald, G.; Mueller, K. T. *J. Chem. Phys.* **2009**, *131*, 144503.

(131) Sarotti, A. M.; Pellegrinet, S. C. *J. Org. Chem.* **2012**, *77*, 6059.

(132) Sarotti, A. M.; Pellegrinet, S. C. *J. Org. Chem.* **2009**, *74*, 7254.

(133) Elena, B.; Emsley, L. *J. Am. Chem. Soc.* **2005**, *127*, 9140.

(134) Elena, B.; Pintacuda, G.; Mifsud, N.; Emsley. L. *J. Am. Chem. Soc.* **2006**, *128*, 9555.

(135) Pickard, C. J.; Salager, E.; Pintacuda, G.; Elena, B.; Emsley, L. *J. Am. Chem. Soc.* **2007**, *129*, 8932.

(136) Glomme, A.; März, J.; Dressman, J. B. *J. Pharm. Sci.* **2005**, *94*, 1.

(137) van Tonder, E. C.; Maleka, T. S. P.; Liebenberg, W.; Song, M.; Wurster, D. E.; de Villiers, M. M. *Int. J. Pharm.* **2004**, *269*, 417.

(138) Cragg, G. M.; Grothaus, P. G.; Newman, D. J. *J. Nat. Prod.* **2014**, *77*, 703.

(139) Altomare, A.; Giacovazzo, C. ; Guagliardi, A.; Moliterni, A. G. G.; Rizzi, R.; Werner, P. E. *J. Appl. Crystallogr.* **2000**, *33*, 1180.

(140) Boultif, A.; Louer, D. *J. Appl. Crystallogr.* **2004**, *37*, 724.

(141) Hofmann, D. *Acta Cryst. B* **2002**, *58*, 489.

(142) Suzuki, K.; Martineau, C.; Fink, G.; Steuernagel, S.; Taulelle, F. *Magn. Reson. Chem.* **2012**, *50*, 159.

(143) Kotecha, M.; Wickramasinghe, N. P.; Ishii, Y. *Magn. Reson. Chem.* **2007**, *45*, S221.

(144) Massiot, D.; Fayon, F.; Capron, M.; King, I.; Le Calvé, S.; Alonso; Durand, J. O.; Bujoli, B.; Gan, Z.; Hoatson, G. *Magn. Reson. Chem.* **2002**, *40*, 70.

(145) Gaussian 09, Revision A.02., Frisch, M. J.; Trucks, G. W.; Schlegel, H. B.; Scuseria, G. E.; Robb, M. A.; Cheeseman, J. R.; Scalmani, G.; Barone, V.; Mennucci, B.; Petersson, G. A.; Nakatsuji, H.; Caricato, M.; Li, X.; Hratchian, H. P.; Izmaylov, A. F.; Bloino, J.; Zheng, G.; Sonnenberg, J. L.; Hada, M.; Ehara, M.; Toyota, K.; Fukuda, R.; Hasegawa, J.; Ishida, M.; Nakajima, T.; Honda, Y.; Kitao, O.; Nakai, H.; Vreven, T.; Montgomery, Jr., J. A.; Peralta, J. E.; Ogliaro, F.; Bearpark, M.; Heyd, J. J.; Brothers, E.; Kudin, K. N.; Staroverov, V. N.; Kobayashi, R.; Normand, J.; Raghavachari, K.; Rendell, A.; Burant, J. C.; Iyengar, S. S.; Tomasi, J.; Cossi, M.; Rega, N.; Millam, J. M.; Klene, M.; Knox, J. E.; Cross, J. B.; Bakken, V.; Adamo, C.; Jaramillo, J.; Gomperts, R.; Stratmann, R. E.; Yazyev, O.; Austin, A. J.; Cammi, R.; Pomelli, C.; Ochterski, J. W.; Martin, R. L.; Morokuma, K.; Zakrzewski, V. G.; Voth, G. A.; Salvador, P.; Dannenberg, J. J.; Dapprich, S.; Daniels, A. D.; Farkas, O.; Foresman, J. B.; Ortiz, J. V.; Cioslowski, J.; Fox, D. J. Gaussian, Inc., Wallingford CT, **2009**.

"For Table of Contents Use Only"

Crystal engineering of pharmaceutical co-crystals: "NMR-crystallography" of Niclosamide co-crystals

David Luedeker,[†] Rebecca Gossmann,[‡] Klaus Langer,[‡] and Gunther Brunklaus*[,†]

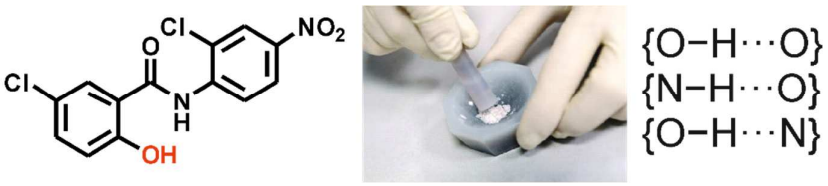

This article reports the crystal structures and solid state NMR characterization of novel co-crystals of the taeniacide niclosamide currently reconsidered for cancer therapy. All samples were obtained

from solvent-assisted solid grinding and studied by PXRD. For niclosamide – 2-aminothiazole, an improved equilibrium solubility was found, suggesting the co-crystal as candidate for future medical treatment.